HIGH-CAPACITY HYPERELASTIC HOLD-DOWN FOR CROSS-LAMINATED TIMBER SHEAR WALLS

By

Oyawoye Abubakar Ajibola

B.Sc., University of Portsmouth, Portsmouth, United Kingdom, 2009
M.Sc., University of Sheffield, Sheffield, United Kingdom, 2012

PROJECT REPORT SUBMITTED IN PARTIAL FULFILLMENT OF
THE REQUIREMENTS FOR THE DEGREE OF
MASTER
OF
NATURAL RESOURCES AND ENVIRONMENTAL STUDIES

UNIVERSITY OF NORTHERN BRITISH COLUMBIA

August 2021

Abstract

Cross-laminated timber (CLT) continues to establish a stronger footing in the Canadian construction industry, also as an option for lateral load resisting systems, such as shear walls. Recent modifications to the Canadian Standard for Engineering Design in Wood (CSA O86-19) allow only rocking kinematics as energy dissipative mechanics for CLT shear walls, whereby hold-down must remain elastic. These provisions necessitate the development of novel hold-down solutions. In this report, the performance of a hyper-elastic high-capacity hold-down was investigated at the component level through tests on: (1) hold-down steel rod, (2) CLT housing, and (3) hold-down assemblies with different sizes of rubber pads. The tests demonstrated that: i) the rubber hold-down can remain elastic under a rocking kinematics provided that the elastic limit of the steel rod is not exceeded; ii) failure of the rod is the subsequent desired ductile mode; iii) the CLT width influences the failure mode; iv) the shape factor influences the achievable deformation of the rubber pad; v) increasing the rubber pad thickness reduces the hold-down stiffness; and vi) increasing the rubber pad width increases the hold-down stiffness. Numerical modelling and optimization suggested that using an intermediate steel laminate between layers of rubber pads could improve its performance. Based on the results of the investigations presented herein, a capacity-design procedure for the hyper-elastic hold-downs was proposed.

Table of Contents

List of Figures

List of Tables

List of Symbols

a_c	Edge distance
a_l	Loaded end distance
h	Height of CLT panel
h_s	Height of the slot
r	Rounded corner radius
w	Width of the CLT panel
w_s	Width of the slot
t	Thickness of the CLT panel
t_l	Thickness of longitudinal layers
t_t	Thickness of transverse layers
w_{lam}	Width of lamellas
w_R	Width of rubber pads
w_{st}	Width of steel plates
d_R	Depth of rubber pads
d_{st}	Depth of steel plates
t_R	Thickness of rubber pads
t_{st}	Thickness of steel plates
φ	Diameter of the centric hole
N_R	Number of rubber layer
CLT	Cross laminated timber
$F_{y,rod}$	Hold-down rod yield load
$F_{d,max}$	Hold-down rod maximum elastic design load
F_{peak}	Hold-down rod peak load
$F_{U,rod}$	Hold-down rod ultimate load
$F_{U,rubber}$	Load in rubber at 40% strain (ultimate load)
$F_{U,CLT}$	CLT Ultimate load
F_{Target}	Elastic design load or Experiment target load
Ro	Reduction factor due to overstrength
Rd	Reduction factor due to ductility
SF	Shape factor
σ_c	Compressive stress in rubber pad
ε_c	Compressive strain in rubber pad
V_{nr}	Compressive Load in rubber pad

Acknowledgements

Glory be to God for the completion of this report.

The completion of this study could not have been possible without the expertise and support of Dr. Thomas Tannert, a remarkable supervisor and mentor. It was a great honor to work with him. His wealth of knowledge provides valuable suggestion for the experiment and review of the report. He is a wonderful person to work with. Many thanks to Dr. Asif Iqbal and Dr. Cristiano Loss for their contribution as co-supervisors and role as committee member. In addition to this, I would like to offer a special thanks to Dr. Asif Iqbal. Without his offer of admission to the program, I would not have a chance to work with Dr. Thomas Tannert.

Many thanks to Hosain Asgari; this study was built on the extensive foundation inherited from his thesis work. Finite element analysis studies carried out was built on parameters derived from his material level testing.

I owe a debt of gratitude to my fellow graduate student, there review and suggestions on my academic writings contributed immensely. I would also like to thank the technical staff at the Wood Innovation Research Laboratory; Michael Billups, Ryan Stern and James Andal, their supports are greatly appreciated. A special gratitude to Claudia Barreira and Mr. Niyi Bankole for their moral support, it was useful throughout my studies.

A final big thank you to my parents, Prof. and Mrs. Oyawoye, my wife, Aisha Nwakego Oyawoye, and children, the contribution of your bravery, patience and mental support is a major part of this success that cannot be understated.

Chapter 1: Introduction

1-1 Background

Environmental concerns around the world have driven the need for sustainable substitutes to steel and concrete multi-storey construction. Cross-laminated timber (CLT) has been proven to be environmentally friendly and sustainable; it acts as a carbon storage and requires less energy to manufacture [1]. CLT has structural properties that makes it suitable for multi-story applications and tackling earthquake-related challenges [2, 3, 4]. When compared with steel and concrete, CLT is lighter and has a higher strength to weight ratio, which results in a smaller foundation and consequently saving project cost and construction time. CLT has gained popularity as a building material in Canada because of these advantages [5]. Many CLT Structures have been erected around Canada in the past decade; examples include the Wood Innovation and Design Centre (WIDC), a 29.5m high 6-storey building in Prince George, British Columbia, the Origine building in Quebec City which is 41m high; and the 18 story UBC Brock Commons Tall Wood House in Vancouver, which is 54m high [6].

1-2 Problem statement

Since wood when loaded in tension or shear is a brittle material, wood structures typically rely on their connections for ductility to avoid brittle failure [7, 8]. Consequently, recent research and development efforts have given more attention to innovation and the manufacture of proprietary connector kits for mass timber construction. Contemporary connectors are usually made of cold-formed steel with various fastener types that can provide the ductility needed in structural design [9, 10]. However, dissipative connections suffer degradation in stiffness and strength during earthquake action, a phenomenon known as pinching action [11].

In any CLT shear wall, the function of the hold-down is to resist uplift from overturning moments caused by lateral forces. Recent modifications in the Canadian Standard for Engineering Design in Wood (CSA O86-19) dictate that hold-downs in CLT shearwall remain elastic, even though hold-downs have been widely proven to act as dissipative connections. The standard also dictates that rocking should be the only form of allowable kinematics [12, 13]. Most of the existing hold-downs cannot accommodate such kinematics and remain elastic at the same time [14]. Therefore, there is a need for innovative hold-down solutions that can meet these new standard requirements.

A hyperelastic hold-down system was developed and investigated by Asgari et al. [15]. Even though the concept is still in its early stage of development, the tests demonstrated that the rubber hold-downs exhibited high strength and deformation capacity without any residual deformation after unloading. Shape factor and loaded area of rubber layers were the main factors that contribute to the response of the rubber hold-down.

The layout of the hold-down in a shear system is as described in Figure 1-1. The concept consists of a coupled shearwall connected by a vertical joint for energy dissipation. The rubber hold-down itself consists of an opening inside the CLT panel with a rubber pad and compression plate, connected to the floor beneath through a steel rod that passes through a drilled hole in the middle of all of the hold-down assembly's members. Rocking kinematics is ensured in the shearwall through a supporting non-dissipative shear connector. When the shear wall rocks, the rod is loaded in tension, compressing the rubber pad as a result.

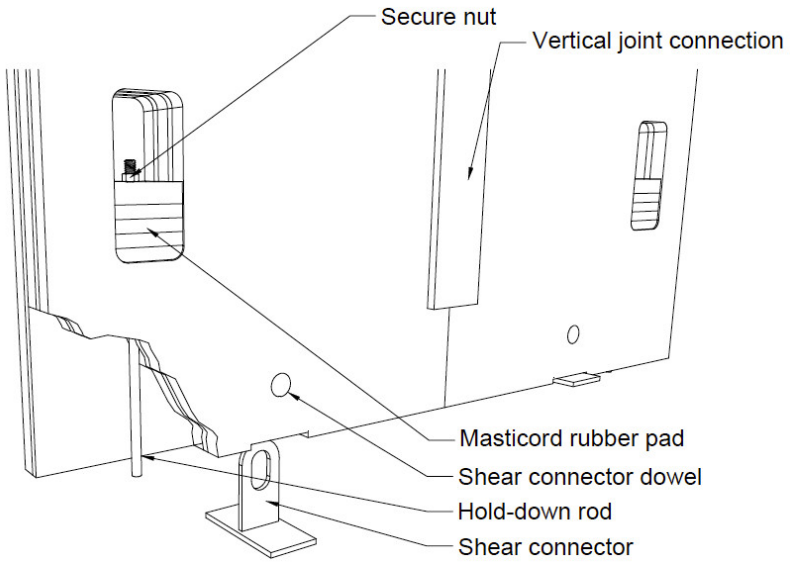

Figure 1-1: Layout of hyper-elastic hold-down in a CLT shear wall

1-3 Objective, scope and limitations

The work presented in this report studied the hyper-elastic rubber hold-down on the component level based on its role in full-scale shearwall system. To achieve this objective, first the yield and ultimate strength of the steel rods were verified. Then, the hold-down system without the rubber pad was tested to failure. Subsequently, the CLT housing was tested to failure to evaluate its brittle failure strength. Conclusively, tensile tests were performed on the hyper-elastic rubber hold-down setup with various rubber thicknesses for a targeted load at various load rates. To complement the experimental study, numerical simulations were carried out to model and optimize the hyper-elastic behavior of different thicknesses of rubber. The result from the numerical analysis was then validated using experimental data.

The study of the full-scale shearwall system was beyond the scope of this study, this research focuses on the behavior and optimization of the hold-down on a component level.

Chapter 2: Literature Review

2-1 Cross-laminated timber

Cross-laminated timber (CLT) is an engineered wood panel product that consists of several layers of lumber boards stacked orthogonally and glued together. Its cross-section has at least three glued layers of boards placed in orthogonally alternating orientation to the neighboring layers. CLT products are usually made up of an odd number of layers with a minimum of three layers and up to seven layers or more. CLT usually comes in a size of up to 3 m in width, with a length of up to 18m. In most cases, its size is limited by transportation regulations. The layers in the minor direction are usually produced using lower-grade lumber. Which can be either visually stress-graded lumber (V grades) or machine stress-rated (MSR) lumber (E grades) [16]. The CLT panel stress grading is usually in line with the stress grades provided in the ANSI/APA PRG 320 standard for performance rated CLT (ANSI/APA, 2018).

CLT has some advantages over other engineering wood products. Its orthogonal cross lamination offers it an improved dimensional stability. This offers the room for prefabrication of wide floor slabs, long single-story walls in platform construction, and tall plate height conditions as in multi-storey balloon-framed configurations. Also, CLT has relatively high in-plane and out-of-plane strength and stiffness properties. This allows the product to be used in a two-way action for floors, similar to that of reinforced concrete slabs [17]. The reinforcement from its cross lamination also offers CLT considerably higher splitting resistance in some types of connection systems. CLT has good thermal insulation and acoustic performance. It also has better performance under various fire conditions, because it can form a thick char cover during a fire for protection. This allows tall mass timber structures to meet building code fire requirements [16].

Structures made up of CLT are usually put together on-site. Prefabricated panels are brought to the site, lifted using cranes and fastened together using mechanical fasteners such as bolts, dowels, self-tapping screws or steel brackets and so on [18]. Its prefabricated nature offers the ability for high precision and fast construction which increased safety and less demand for skilled workers on-site, less noise, less wastage, timesaving, and cost-saving [16]. For example, the 8-storey The Murray Grove, built in London in 2010, was completed by four people in 27 days [19].

CLT also has a high strength to weight ratio compared to steel or concrete. This results in a lighter superstructure, which means that foundations can be smaller when compared with concrete or steel structure, which consequently saves cost [20]. CLTs are used in construction mostly in the form of wall and floor panels. For wall panels, CLT is usually erected so that the major axis is in the vertical orientation to take vertical loading. As for floor application, CLT can be one-way spanning or two-way spanning depending on its thickness. There are two ways in which CLT multi-structures can be constructed. They are platform-type construction and balloon framing [21]. The provisions provided in the CSA O86 and National Building Code of Canada (NBCC) are tailored for Platform-type constructed CLT Structures.

2-2 CLT shearwalls and connections

In order to achieve taller wood structures, efforts are being devoted towards developing new innovative wood applications, and construction methods that can facilitate engineering design solutions that ensure reliability within capacity-based design method. In the past decade, most attention has been focused on the mechanical performance of timber structures, even though there is insufficient data on its performance in an actual earthquake scenario. Full-scale CLT multi-story shake table test has shown that that midrise CLT structures will perform well under

seismic instances. For example, the 7-story SOFIE project conducted in 2007 at the Hyogo Earthquake Engineering Research Center in Miki, Japan. There, a 13.5 m x 7.5 m and 23.5 m high CLT building designed in accordance with the equivalent static force procedure in the Eurocode 8 was tested. The structure was subjected to different three-dimensional ground motions of various intensities. The earthquake produced a maximum interstorey drift of 1.3%. However, studies have suggested adding ductile elements to CLT building design may further improve building performance [5]. Also, a three-story CLT house shake table test conducted at the NIED laboratory in Tsukuba, showed that CLT can withstand multiple earthquakes with minimal damage [3, 4, 18, 21].

When a platform-type CLT building is subjected to an earthquake loading, the response of the building transfers load through the floor diaphragm and is distributed to the shearwalls. The shearwall is responsible for resistance and energy dissipation in the structure [4]. Full-scale shearwall test and full-scale shearwall numerical analysis carried out by Popovski et al. and Izzi et al., respectively, demonstrated that kinematics is crucial for energy dissipation to occur in CLT shearwall [22, 18]. For a coupled CLT shearwall system described in Figure 2-1, typically comprises two CLT panels connected by a vertical joint, horizontal shear resisting connectors, and hold-downs. CLT panels are considered rigid in a CLT shearwall system. Therefore, lateral stiffness, strength and kinematics in the structure are determined by the properties of connections.

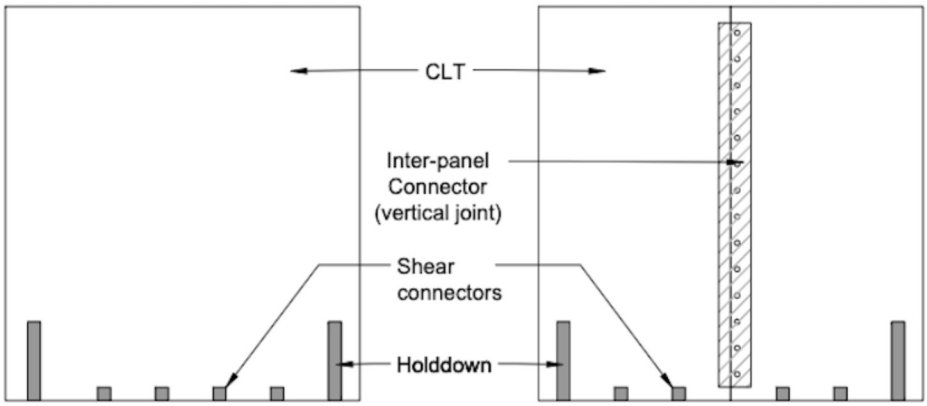

Figure 2-1: Typical CLT shear wall layouts

Coupled CLT shearwall can behave either like a single wall or coupled walls depending on the stiffness of the hold-down in relation to the vertical joint as described in figure 2-2 [22, 23, 24, 25]. Studies have shown that inter-panel connections did not compromise the performance of the building in terms of resistance, however, it increased the overall building deformability [4, 12, 26]. The studies by Izzi et al. and Casagrande et al. and Shahnewaz et al., showed that aspect ratio contributes significantly to the kinematic behavior of the panels and subsequently the amount of force that goes into hold-down [18, 24, 27]. The kinematics interaction of the panels as a single or couple wall behavior is highly influenced by the stiffness of the hold-down and the vertical joint, relative to one another and the aspect ratio of the panels [24, 28].

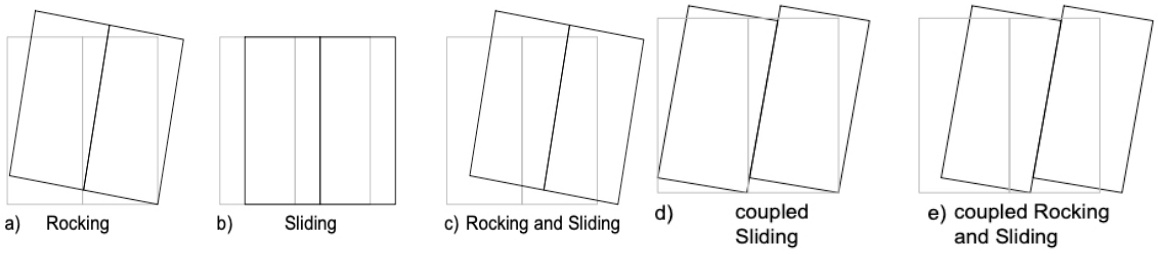

Figure 2-2: Coupled panel kinematic behavior

When an earthquake occurs, damage is inevitable; it provides supplementary energy dissipation. To ensure adequate performance in a building, capacity design is usually employed. Specific connecting elements in the system are required to have enough ductility and deformability for dissipation of energy (dissipative connection), while the remaining connections and structural components are designed with sufficient overstrength to remain elastic (non-dissipative connection) under the rocking as the predominant kinematic behaviour of the shearwall [6]. For CLT shearwalls, the CLT panels are considered rigid, ductility and dissipation are designated to connections in the form of yielding and bending of metal fasteners and connector plates, and wood crushing due to nail embedment [29, 30].

As a requirement for dissipative connections in accordance with CSA O86-19; dissipative connection should be designed such that yielding mode governs the resistance. It should also be at least moderately ductile in the directions associated with the rocking rigid body motions of CLT panels. Finally, such types of connections should possess sufficient deformation capacity under the force and displacement demands that are induced in them to allow for the CLT panels to develop rocking motion [21].

Non-dissipative connections on the other hand are usually provided with sufficient capacity to remain elastic when the dissipative connection reaches ultimate resistance. In the CSA O86-19, the force exerted in the non-dissipative connection when the 95th percentile of ultimate resistance of the dissipative is attained must be less than the 5^{th} percentile elastic limit of the non-dissipative connection. For the CLT panel, the seismic design force may be determined using $R_d R_o = 1.3$ [6, 16, 21, 24, 31].

Prior to the recent update of the O86-19 on CLT shearwall design, non-dissipative connections included floor to wall connection (hold-downs), floor to floor panel and vertical joints between

octagonal panel. In the CSA O86-19, hold-down connections were included as a non-dissipative connection, therefore required to remain elastic throughout an earthquake action.

The role of the hold-downs is to resist uplift resulting from an overturning moment. Previous studies have shown that proprietary connectors such as Simson and MiTicon brackets and other innovations such as HSK can easily meet the amount of load demand elastic [9, 10, 22, 31, 32]. However, such connections deform non-elastically and suffer pinching action under cyclic loading because they do not have the required elastic deformability. Nevertheless, ductility provided by such hold-downs has been proven to satisfy structural performance criteria, as shown by e.g. Popovski et al., on a 3-D system behavior of CLT structures under lateral loads using a two-story full-scale of a CLT structure, a 2-storey structure of 6.0 m by 4.8 m in plan and with a total height of 4.9 m. The study concluded that the presence of additional hold-downs lowered the uplift deformations of the walls but did not increase the building's resistance [18].

2-3 Hyper-elastic rubber hold-down

A hyperelastic hold-down system was developed and investigated by Asgari et al. [15]. It consists of Masticord elastomeric rubber (MER), compression plate(s) and steel rod. Masticord rubber is a composite material consisting of an elastomer with random-oriented synthetic fibers. It is an isotropic material that behaves in a non-linear manner. For a shearwall system that uses such type of hold-down, the tension force that occurs in the hold-down when the shearwall rocks is translated into a compression load exerted by the top plate on the rubber pad. This causes the rubber pad edges to bulge, and its surface area increases. The hold-down boundary restriction allows only two opposite faces to bulge due to its assembly position in the CLT housing compartment.

The shape factor (SF) has been shown to contribute significantly to the strength and stiffness of the MER pad. The size, and boundary condition influences the shape factor. The SF for a rectangular pad with a cylindrical hole at the middle can be estimated using the following formula provided in the MER manufacturers design guide [33]:

$$SF = \frac{d_R w_R - \frac{\pi\phi^2}{4}}{2((d_R + w_R) - \pi\phi)t_{R,t}} \qquad (2\text{-}1)$$

Where d_R w_R $t_{R,t}$ and Φ are Depth of rubber pads, Width of rubber pads, Thickness of rubber pads and Diameter of the center hole at the middle of the rubber respectively.

In rubber hold-down applications, the role of the rubber pad is to resist compression only. The synthetic fibers in the rubber pad strengthen the elastomer [15, 33]. Based on the manufacturer, Masticord rubber is assumed to reach its ultimate load at 40% compressive strain deformation. Based on the manufacturer's guide, at 40% compressive strain, the reinforcement fibers debond and pull away from the exterior surface of the pad. The voids left by the de-bonded fiber start to experience tears in the elastomer. A tear may also occur in the fibers leading to permanent deformation. At this stage, the edges are where most damage is concentrated for the pad, depending on the amount of strain in such instances. Further deformation beyond this limit will typically extend from the situation of the previous damage to areas having the highest strain. However, unlike other materials, the rubber pad will continue to transfer and distribute load after it is damaged [33].

Asgari et al. [15] tested the rubber hold-down concept with a thickness of 1” and 2” enclosed in a CLT opening. A total of 53 quasi-static monotonic and cyclic tests were performed and demonstrated that rubber hold-downs exhibited high strength and deformation capacity

without any residual deformation after unloading. The shape factor and loaded area of rubber layers were found as the main factors that contributed to the response of the rubber hold-down. It was shown that openings wider than the lamellas' width weakens the CLT and will leave the panel susceptible to brittle failure. The need for further research using a thicker rubber pad in the hold-down was suggested. The study also suggested using laminated rubber bearings in between the pad layer rather than the plain rubber. The study claimed that rubber bearing can provide higher stiffness in the rubber Hold-down.

2-4 Summary

While CLT has been proven to be an efficient and sustainable material for wood structures, the concerns around recent modification in CSA O86-19 for hold-downs to remain fully elastic during earthquake action calls for more research on CLT hold-down design. This is to provide a solution that satisfies the new requirement because studies have shown that proprietary hold-downs cannot facilitate rocking and remain elastic. The hyper-elastic rubber hold-down concept has shown significant potential as a feasible solution to address this problem but more research is deemed necessary to improve its performance and develop capacity-design principles.

Chapter 3: Experimental investigations

3-1 Overview

Even though CSA 086-19 recommends that hold-downs in CLT shearwalls should remain elastic during dynamic action, it is good practice that failure after overloading is ductile. This will provide energy dissipation and avoid sudden brittle failure that may be catastrophic. Consequently, it is essential that the failure of the system occurs in the steel rod and not the rubber or CLT panel which should both have a higher load-bearing capacity than the hold-down steel rod, so that the failure of the system will occur in the hold-down rod.

The completed tests provided a stage-by-stage guidance for the component level capacity design of the rubber hold-down in a shearwall system. In other to demonstrate how brittle failure can be avoided in the hold-down even if failure were to occur. For this study, two levels of protection were considered (see Figure 3-1).

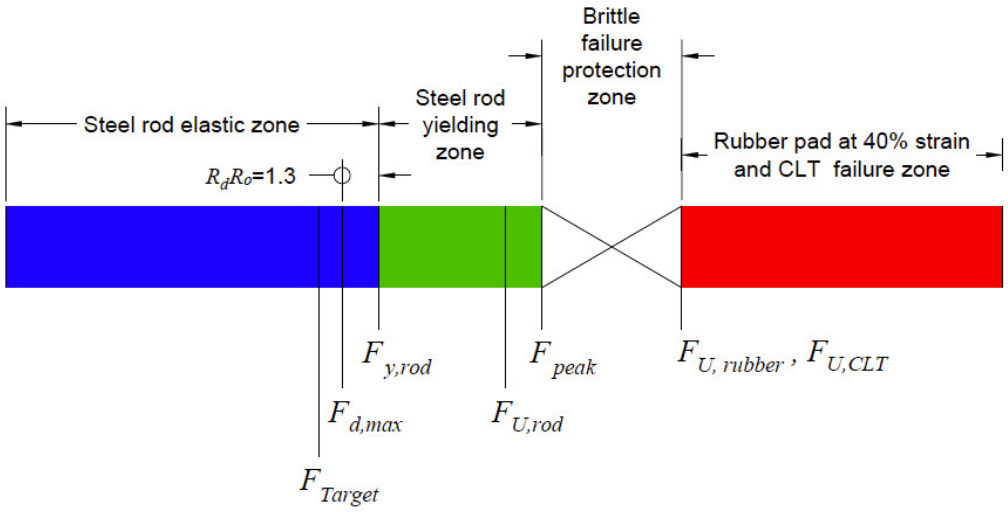

Figure 3-1: Capacity-based design principle

The first protection avoids failure of the CLT and prevents the rubber pad from exceeding its ultimate strain capacity of 40%. This was achieved by ensuring sufficient brittle failure safety margin between the peak load of the steel rod F_{peak}, and the failure load of the CLT $F_{U,CLT}$ and rubber pad $F_{U,\,rubber}$. The second protection applies an overstrength factor R_dR_o of 1.3 to ensure that the hold-down remain elastic throughout the experiment.

In order to achieve the study objective, a series of quasi-static monotonic tensile tests were first carried out on a sample of three (3) different rod diameters; 4/3" (full cross section), 10/16" and 9/16". The objective of these tests was to identify a suitable elastic limit for the hold-down test by defining the 5th percentile and 95th of the yield and ultimate strengths. Then, quasi-static monotonic and a modified CUREE cyclic test was carried out on a total of six (6) samples of the selected hold-down rod to study its fatigue resilience. Subsequently, the CLT housing was loaded in tension to study the brittle failure of the panel under a quasi-static monotonic loading. This is to ensure the CLT housing is well protected above the 95th percentile of the steel rod ultimate tension strength. Finally, a comprehensive test series was carried out on the full hold-down system using ten different sizes of Masticord rubber pad. Each test sample subjected to a monotonic tensile target load at various loading rates.

3-2 Materials – steel rods

Steel rods, grade 8 was used, the yield and ultimate strengths of the steel rod was determined in a preliminary test carried out. A diameter of 19.1 mm (¾") was chosen. For the preliminary tests, four samples of the full ¾" rod, and four samples each of lathed dog bone sample of diameter 10/16" and 9/16" were tested on 300mm long specimens. Subsequently, a hold-down steel rod tests were carried out on a 600mm full rod of the same diameter. Full size sample of the rods used in the study is illustrated in Figure 3-2.

Figure 3-2: Steel rod samples

3-3 Materials – CLT

The CLT samples were 5-ply 139mm E1M4 grade by Structurlam, with 35mm MSR E-rated lumber in all major strength direction layers and 17mm SPF #2& Btr lumber in the minor axis. The CLT used was manufactured in accordance with PRG 320-2012 requirements. The material property of the CLT is described in Table 3-2.

Table 3-1: The material property of the CLT sample

CLT	Grade	Longitudinal layers					Transverse layers				
		E	f_t	f_c	f_{cp}	f_s	E	f_t	f_c	f_{cp}	f_s
139E	E1M4	12400	17.7	19.9	6.5	0.5	9000	3.2	9	5.3	0.5

The CLT is the main housing compartment for all other members in the setup for the experiment. The CLT panel sample was prepared with a rectangular opening large enough to accommodate symmetrical assembly setup for the hold-down experiment. The opening was also prepared with rounded edges with a radius *r* on all corners to prevent concentrated stress. A hole was drilled through the center of each panel on the face perpendicular to the grain direction of the outermost layer, linking the end side of the panel of the rectangular opening prepared in its middle. This provided the passage for fixity on both sides. The geometry of the CLT housing is provided in Figure 3-3 and in Table 3-3. These can be categorized into group A and group B.

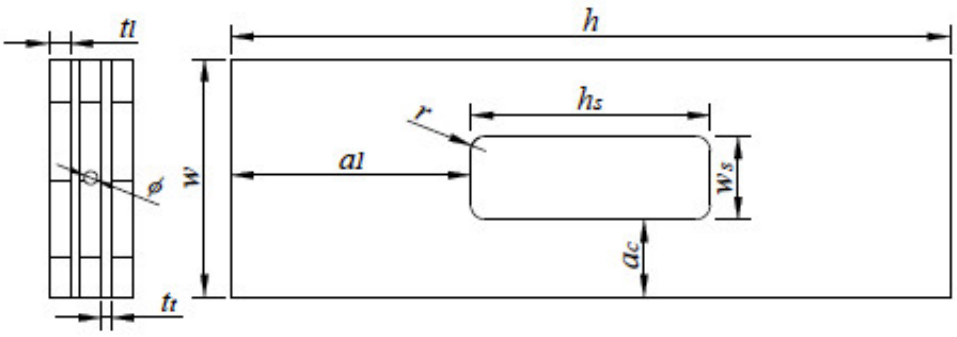

Figure 3-3: Geometry parameters for CLT housing

Table 3-2: Dimension of CLT samples

Group	CLT panel dimension					Slot dimension		a_l	a_c	d_c	w_{lam}	r
	h	w	t	t_l	t_t	h_s	w_s					
A	1000	500	139	35	17	350	90	500	205	22	130	5
	1000	500	139	35	17	350	140	500	180	22	130	5
B	1200	400	139	35	17	400	90	600	155	22	130	25
	1200	400	139	35	17	400	140	600	130	22	130	25

3-4 Materials – rubber

Masticord elastomeric rubber (MER) pads were used for the study (Figure 3-3). The chosen widths of the rubber pad determine the dimension of the prepared CLT opening. Masticord elastomeric rubber is a composite material consisting of elastomer (made up of carbon black, zinc oxide, sulphur, rubber processing oils, and other chemicals encapsulated in the rubber crumb) with random oriented synthetic fibres. It was selected for its high compressive strength, cost-effectiveness, and commercial availability in comparison to other elastomeric rubber materials. Its role in the setup of the rubber pad is used to resist uplift through compression as later demonstrated. Relevant mechanical properties of Masticord are listed in Table 3-4. The

stress-strain relationship for the rubber pad can be predicted using an empirical formula based on MER manufacturers design guide [33]:

$$\sigma_c = 0.00689(0.6SF + 2)\varepsilon_c^{1.8} \qquad (3\text{-}1)$$

Where, σ_c and ε_c are the vertical compressive stress and strain on the rubber pad without any rotation or horizontal displacement. The maximum allowable load V_{nr} and compressive stress σ_c for all samples are hereby listed in Table 3-4. This is based on a maximum strain value of 40% as recommended by the manufacturer.

Table 3-3: Relevant mechanical properties of Masticord [33]

Compression e_{max}	40% maximum compressive strain
Shear	75% maximum compressive strain
Creep	irrelevant after application of load
Shape factor	Limited by 40% maximum compressive strength
Slip friction	coefficient 0.7 - 0.9 (by static incline plane)
Maximum compressive stress	55.16MPa
Tensile Strength (ASTM D 412, Die B)	6.89 MPa

Rubber pads of thickness one, two, three and four inch were produced by gluing multiple layers of the 1" (t_R) MER pad. A fifth thickness was later included by combining 1" and the build-up glued 4" MER pad. N_R represents the total number of Layers (Figure 3-4). Figure 3-4 demonstrates the bulging behavior of the rubber pad under compression. For the setup that was used, the breath of the sample d_R was restricted from bulging by the CLT enclosure. A 22mm diameter hole was drilled at the middle of each pad for support fixity. A total of 10 different sample types were prepared by cutting out a 90 x 140 mm^2 (see Figure 3-5a) and a 140 x 140

mm^2 (see Figure 3-5b) rectangular cuboid of each of the buildup MER pad types. The geometrical details and SF of each sample is listed in Table 3-5.

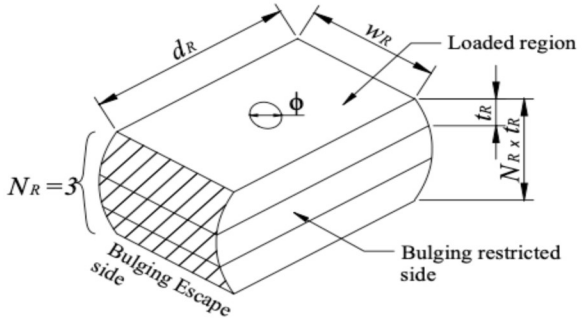

Figure 3-4: Geometry parameters of rubber pad

Where, d_R, w_R, and $t_{R,t} = t_R \times N_R$ are the depth, width, and thickness of rubber pads, respectively.

a)

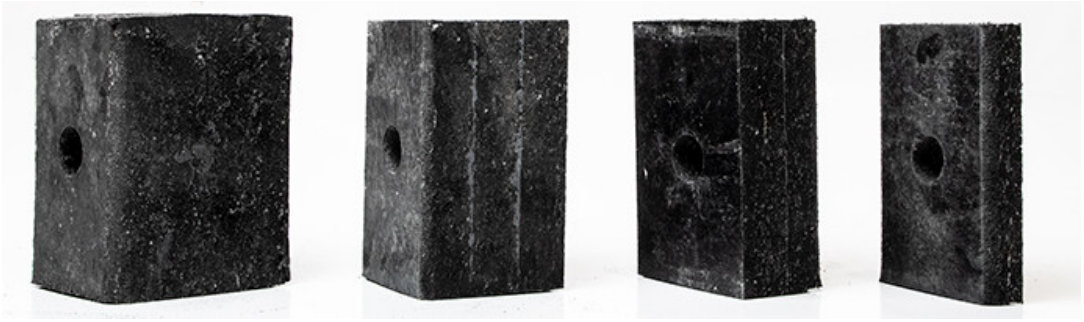

b)

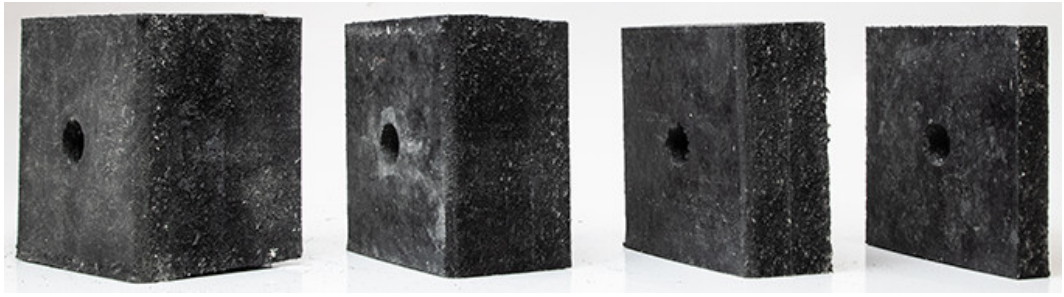

Figure 3-5 Masticord rubber pad a) 90mm pad b) 140mm pad

Table 3-4: Rubber test samples dimension

Thickness	d_R	w_R	t_R	N_R	$t_{R,t}$	φ	SF	V_{nr}	σ_c
[inch]	[mm]	[mm]	[mm]	[mm]	[mm]	[mm]		KN	MPa
1"	140	90	25.4	1	25.4	22	1.9	209.9	17.18
2"	140	90	25.4	2	50.8	22	1.0	171.4	14.03
3"	140	90	25.4	3	76.2	22	0.6	158.6	12.98
4"	140	90	25.4	4	101.6	22	0.5	152.2	12.45
5"	140	90	25.4	5	127.0	22	0.4	148.3	12.14
1"	140	140	25.4	1	25.4	22	2.2	341.2	17.75
2"	140	140	25.4	2	50.8	22	1.1	274.0	14.26
3"	140	140	25.4	3	76.2	22	0.7	251.6	13.09
4"	140	140	25.4	4	101.6	22	0.5	240.4	12.51
5"	140	140	25.4	5	127.0	22	0.4	233.7	12.16

3-5 Materials: top and bottom plate

The dimensions of the top and bottom plates are illustrated in Figure 3-6. The top plate was over-designed with a thickness of 2” to ensure that no local deformation occurred. The bottom plate was trimmed with a rounded edge of the same radius as the rounded corner of the CLT housing, this is to allow an even stress transfer to the corners of the CLT panel housing. Both top and bottom plates were fabricated with a hole of 22mm in diameter at the center to allow room for fixity.

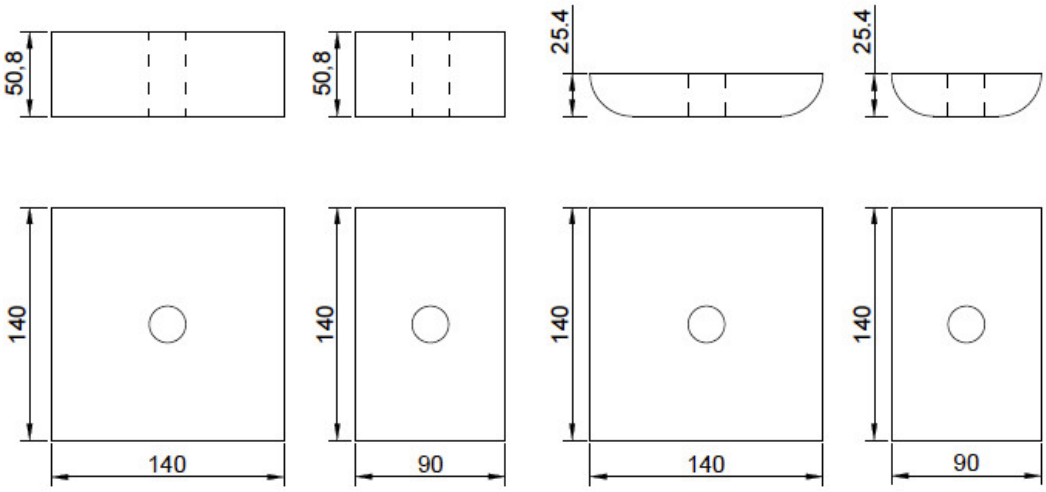

Figure 3-6: Steel top and bottom plates

3-6 Steel rod tests

A preliminary monotonic tensile test was first carried out on the high strength and high yield threaded 3/4" steel rods to be used as the hold-down steel rod. For the test, a total of 12 samples consisting of 3 different diameter sizes were tested. Each specimen first was measured with a vernier digital caliper before being testing. Specimens were attached to hydraulic collett grips of a UTM machine and loaded in tension at 10mm/min till failure was achieved. All deformation was recorded relative to the actuator position.

Since the hold-down steel rod may also be susceptible to strength degeneration due cyclic loading, the fatigue behavior of the hold-down system without any rubber pad was tested. To carry out this test, the 22mm hole drilled into the CLT samples was widened to 30mm. The holes in the bottom plates were also widened to 1" to ensure free passage. A high strength 1" steel rod was used to secure the CLT to the UTM machine on one end, while the proposed hold-down rod was secured to the other end of the CLT housing. The test setup is illustrated in Figure 3-7.

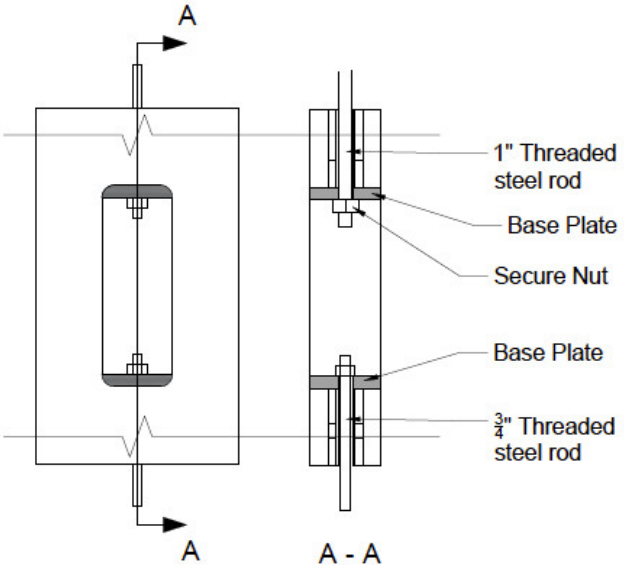

Figure 3-7: Layout for hold-down steel rod tests

Quasi-static monotonic and cyclic tests were conducted on a total of six (6) samples. Three (3) of the hold-down rod specimens were first tested to failure using a displacement controlled monotonic tensile loading protocol at a loading rate of 10mm/min. After that, a tensile cyclic load test was conducted using the remaining three (3) specimens. A modified version of CUREE method C in accordance with ASTM E2126 was used [34], see Figure 3-8. The target displacement was calculated based on the initial monotonic test as 35mm. It is worth mentioning that deformation was acquired straight from machine-reading and not an LVDT. Therefore, the acquired deformation is the overall deformation of the hold-down system without the rubber pad.

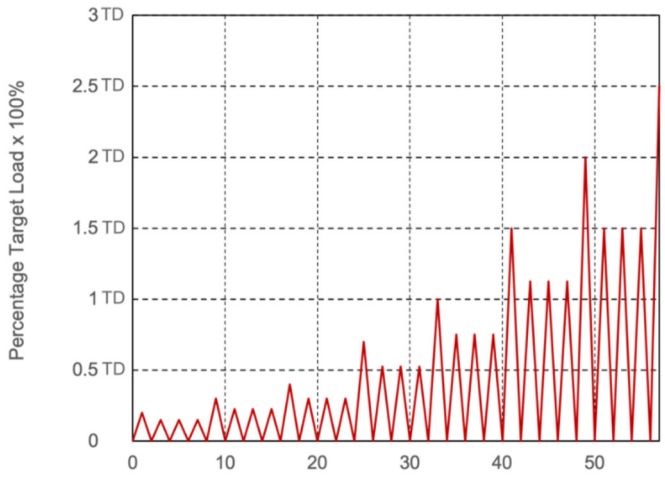

Figure 3-8: Modified CUREE cyclic loading

3-7 CLT tests

Quasi-static monotonic tensile tests were carried out on the CLT housing samples. Each sample was loaded to failure, at a loading rate of 5mm/min. The setup of the test is similar to the hold-down steel rod test setup, but with a 1" threaded steel rod used on both sides as shown in Figure 3-9 and summarized in Table 3-6.

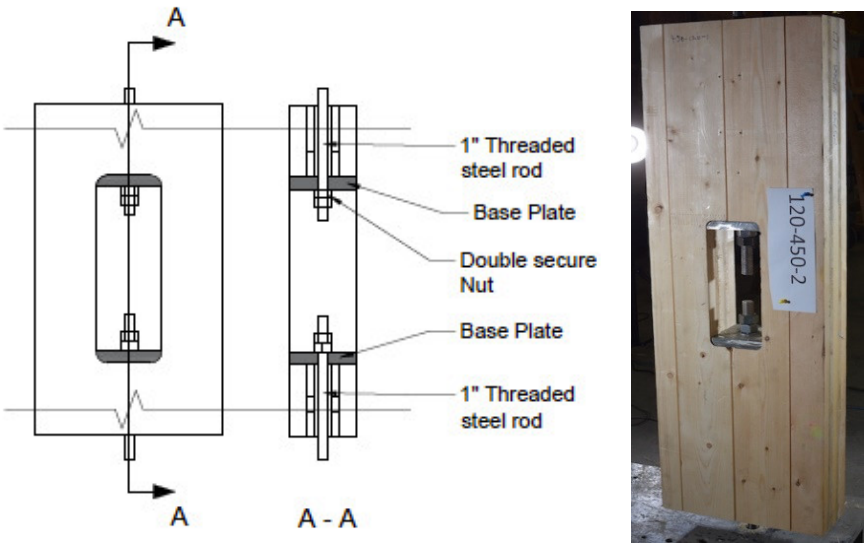

Figure 3-9: CLT test setup

Table 3-5: Labels and dimensions for the CLT test sample

Label	w_s	m
90-350-1	90	350
90-350-2	90	350
90-370-1	90	370
90-400-1	90	400
90-400-2	90	400
120-450-1	120	450
120-450-2	120	450
140-370-1	140	370
140-400-1	140	400

3-8 Hold-down tests

The different layout configurations used in the experiment are described in Figure 3-10. The first Layout, cf. A, uses only a top plate that compresses the rubber pad to the CLT support. This leaves the CLT outer layer vulnerable to delamination from the bulging, leading to premature failure of the CLT compartment. The second Layout, cf. B, used a bottom plate solely to protect the CLT compartment. The third Layout, cf. C, used only one hold-down with the 5" thick rubber pad. Average relative deformation in the rubber pad sample was recorded in reference to the top plate during each test using Linear Variable Differential Transformers (LVDT) devices. The LVDT were secured to the CLT and labeled as described in the Figure 3-10 below for each layout.

The hold-down test was set up to isolate the behavior of the rubber hold-down to study how certain parameters influence the performance. The parameters of interest were: 1) the rubber

thickness; 2) the rubber width; and 3) the loading rate. Thus, ten rubber samples were tested using the setups described in Figure 3-10. Tension load was applied using a displacement control universal testing machine (UTM) with a capacity of 500kN. A tensile monotonic displacement-controlled target load F_{Target} of 120kN was applied to each specimen at a loading rate of 10mm/min. It is worth noting that an initial preload of 5kN was introduced to the setup system by applying a torque of 35lbs on the nut on the inside of the CLT opening before each test. This is to ensure a consistency in the tightening of the all sample. Deformation of the MER pad due to the compression load applied on the MER pad was recorded at 120kN. The target load was decided based on the preliminary steel rod tests so that the applied load was less than a factored average yield load with a R_dR_o factor of 1.3 to ensure that the steel rod remained elastic throughout the test. All tests were repeated three (3) times for each experiment. The label for each test is detailed in Table 3-7.

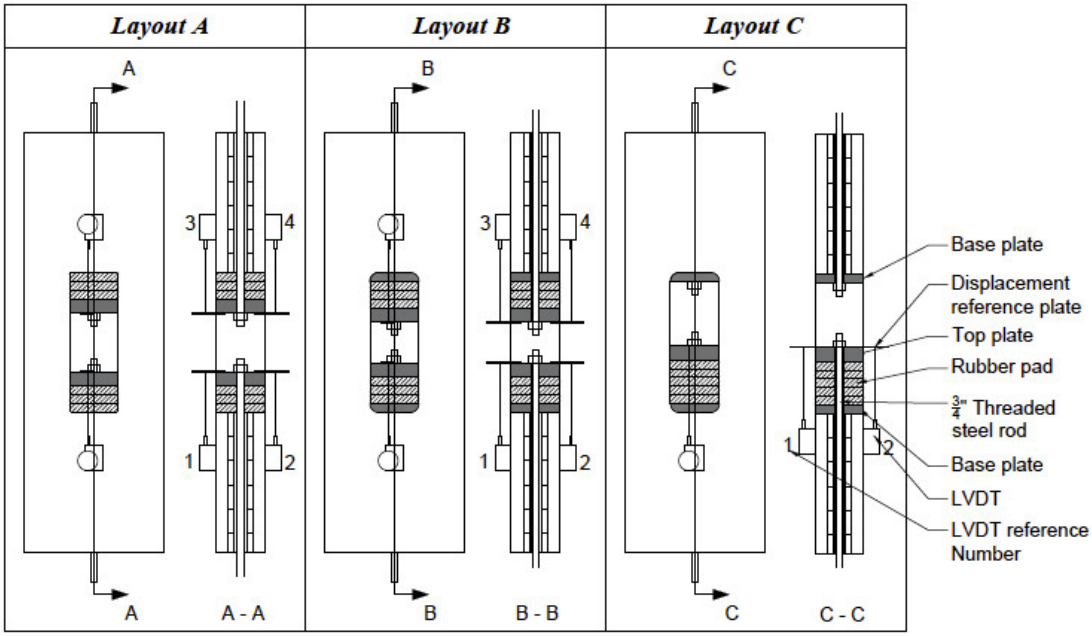

Figure 3-10: Rubber hold-down component level test setups

Table 3-6: The label, discretion and loading rate for the hold-down test.

Depth	Width	Thickness	Rate of loading	Label
[mm]	[mm]	[inch]	[mm/min]	
140	90	1"	10	90-1-10
			50	90-1-50
			250	90-1-250
		2"	10	90-2-10
			50	90-2-50
			250	90-2-250
		3"	10	90-3-10
			50	90-3-50
			250	90-3-250
		4"	10	90-4-10
			50	90-4-50
			250	90-4-250
		5"	10	90-5-10
			50	90-5-50
			250	90-5-250
	140	1"	10	140-1-10
			50	140-1-50
			250	140-1-250
		2"	10	140-2-10
			50	140-2-50
			250	140-2-250
		3"	10	140-3-10
			50	140-3-50
			250	140-3-250
		4"	10	140-4-10
			50	140-4-50
			250	140-4-250
		5"	10	140-5-10
			50	140-5-50
			250	140-5-250

Chapter 4: Experimental results and discussion

4-1 Steel rod test results

The load-deformation curves from the steel rod tests are presented in the Figure 4-1. Figure 4-1a and Figure 4-1b show the curves of the monotonic test from the preliminary tests and Figure 4-1c and Figure 4-1d illustrate the curves of the fatigue test carried out. The result of the preliminary test is presented in Table 4-1. Also shown in Table 4-2, are the peak loads F_{Peak}, yield loads $F_{y,\,rod}$, yield elongations $d_{y,Rod}$, and fracture elongation $d_{ult,Rod}$, generated from the fatigue test carried out. Ductility μ_{Rod} was calculated in accordance with ASTM E2126 [30].

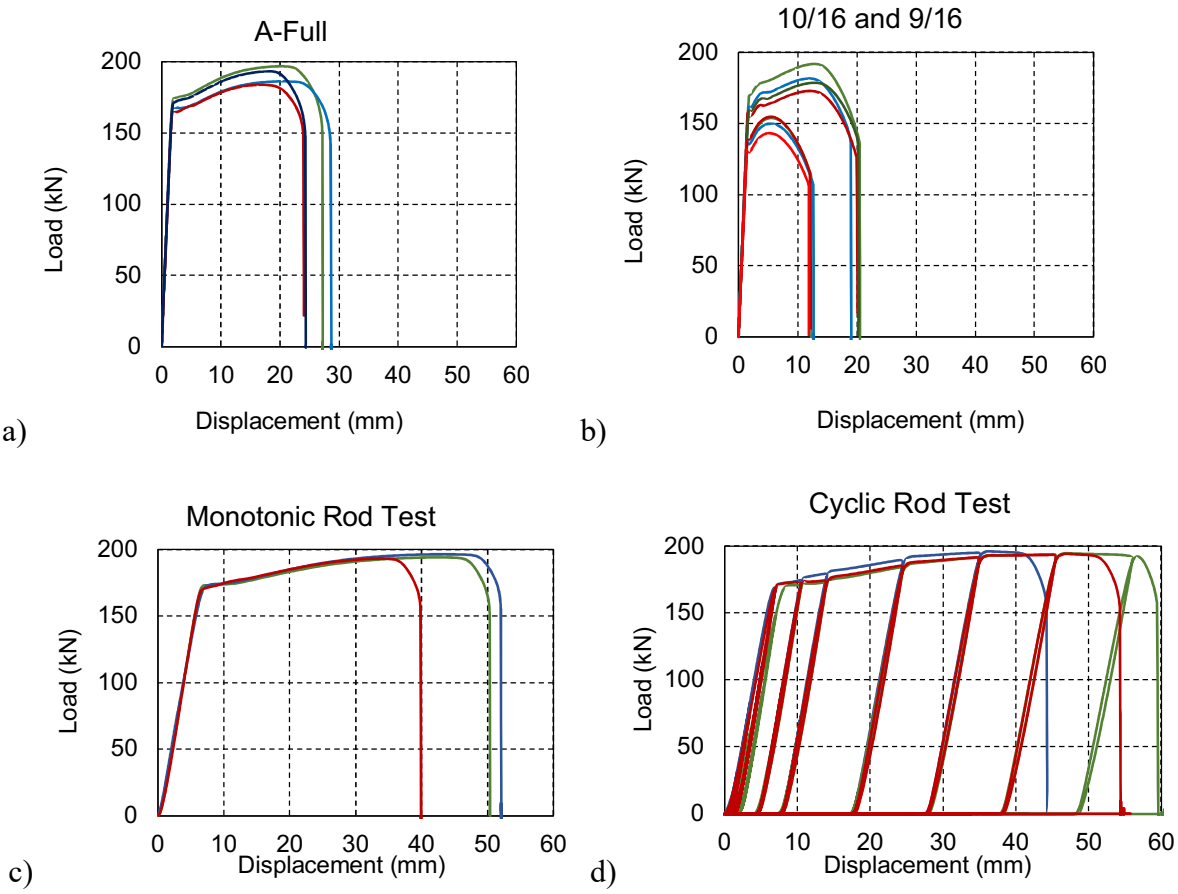

Figure 4-1: Load-displacement of a) full and b) section reduced rod under monotonic loading; c) preliminary test carried and d) hold-down rod quasi-static monotonic and cyclic test

Table 4-1: Result of preliminary steel rod test

Specimen	Diameter (mm)				Yield strength KN	Yield stress MPa	Peak strength KN
	Top	Middle	Bottom	Average			
A-full	18.9	18.9	18.9	18.9	162.0	-	183.8
B-full	18.9	18.9	18.9	18.9	171.4	-	193.3
C-full	18.8	18.9	18.8	18.8	163.5	-	186.3
D-full	18.9	19.2	18.7	18.9	170.9	-	196.8
A-10/16	15.9	15.9	15.9	15.9	153.1	1297	173.0
B-10/16	15.9	16.0	16.0	16.0	156.5	1285	178.7
C-10/16	15.9	15.9	15.9	15.9	158.9	1250	181.8
D-10/16	15.9	15.9	15.9	15.9	168.1	1181	192.0
A-9/16	14.0	13.8	13.9	13.9	138.0	1100	154.8
B-9/16	14.3	14.3	14.3	14.3	129.0	1245	143.3
C-9/16	14.3	14.3	14.1	14.3	134.8	1192	150.0
D-9/16	14.3	14.3	14.3	14.3	137.2	1171	154.0

Table 4-2: Results of hold-down rod quasi-static monotonic and cyclic tests

Loading	F_{Peak}	$F_{y,Rod}$	$0.8F_{peak}$	$d_{y,Rod}$	$d_{ult,Rod}$	μ_{Rod}
	[kN]	[kN]	[kN]	[mm]	[mm]	
Monotonic	196.3	170.5	157.1	6.9	51.0	7.4
Monotonic	194.0	170.7	155.2	6.5	49.5	7.6
Monotonic	192.0	167.5	153.6	6.3	39.0	6.2
Cyclic	194.2	170.0	155.3	7.1	54.0	7.6
Cyclic	195.1	169.8	156.0	7.1	43.5	6.1
Cyclic	194.6	168.6	155.7	8.2	58.6	7.1

4-2 CLT test results

From the monotonic tensile test carried out to study the strength of the CLT housing, the load-deformation curve from the study is shown in Figure 4-2. Table 4-3 presents the peak load $F_{CLT,peak}$ and deformation at peak load $d_{CLT,ult}$.

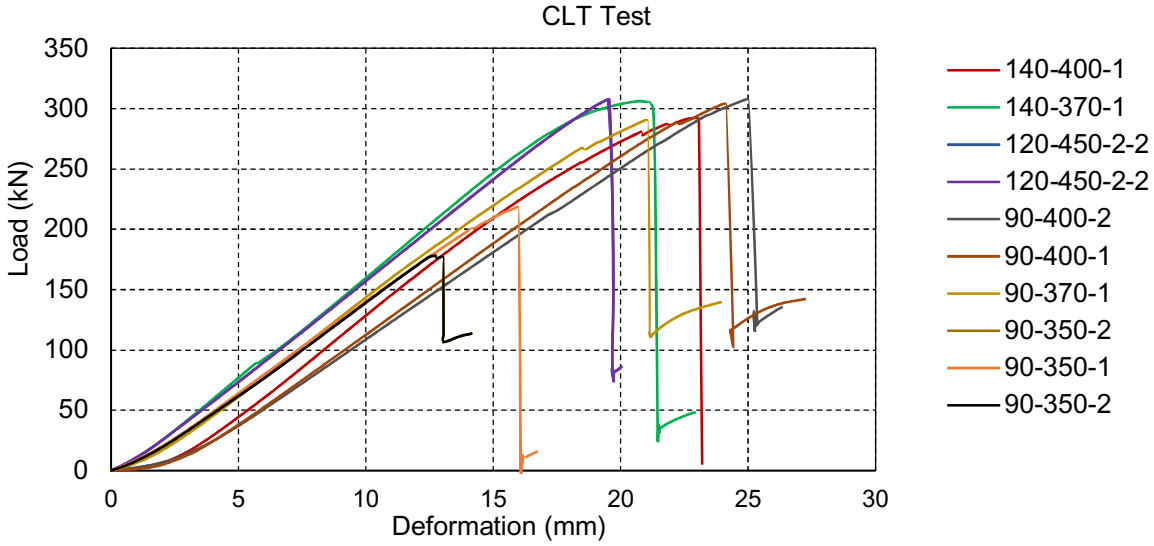

Figure 4-2: CLT test load-displacement curve

Table 4-3: CLT test results

Label	w_s	a_l	$F_{CLT,peak}$	$d_{CLT,ult}$	k_{CLT}
	[mm]	[mm]	[kN]	[mm]	[N/mm]
90-370-1	90	370	291.5	20	16405
90-400-1	90	400	304.7	24	14984
90-400-2	90	400	308.6	25	14445
120-450-1	120	450	303.6	22	15680
120-450-2	120	450	308.7	20	16522
140-370-1	140	370	280.7	18	16376
140-400-1	140	400	292.5	23	16819
90-350-1	90	350	177.8	13	14390
90-350-2	90	350	219.5	16	15413

4-3 Hold-down test results

Figure 4-3a and Figure 4-3b shows the load-deformation curve of the 90mm and 140mm wide rubber hold-down. The average deformations recorded in the rubber pad from the two LVDTs attached to both sides for the top and bottom sample at the target load (F_{tar} = 120kN) are shown in Table 4-4.

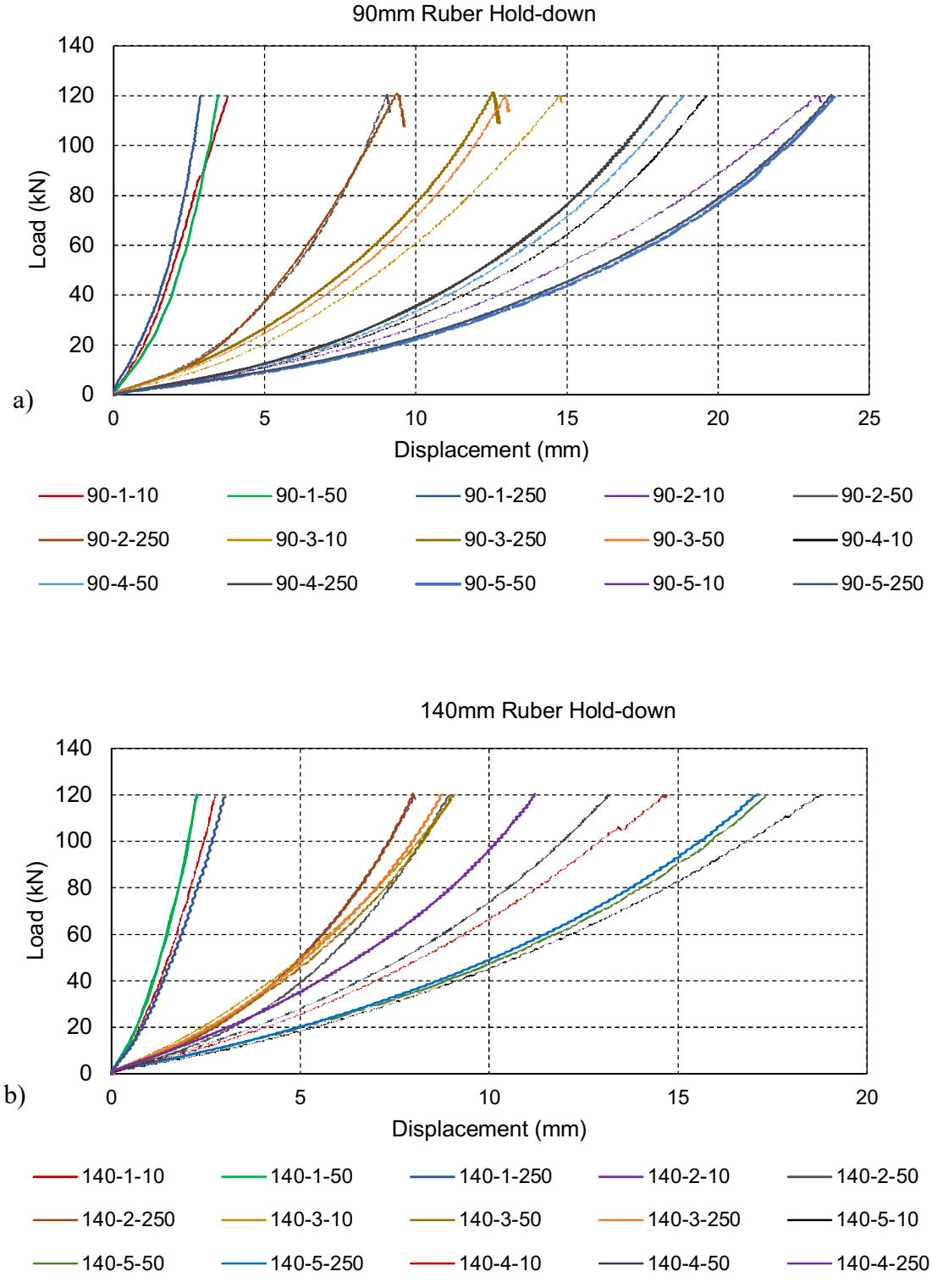

Figure 4-3: Hold-down load-displacement: a) 90mm and b) 140mm wide rubber hold-down

Table 4-4: Hold-down deformation under quasi-static monotonic loading

Width	Thickness	Speed	A top	A bot	B top	B bot	Strain
[mm]	[inch]	[mm/min]	[mm]	[mm]	[mm]	[mm]	
90	1"	10	3.8	4.0	4.0	4.4	16%
		50	4.1	3.5	3.3	3.4	14%
		250	2.9	2.4	3.2	3.3	11%
	2"	10	9.4	9.5	9.3	9.5	19%
		50	7.0	6.6	9.0	9.2	16%
		250	7.4	10.3	8.8	9.3	18%
	3"	10	16.0	15.7	14.8	15.5	20%
		50	15.3	14.4	12.9	13.2	18%
		250	14.5	13.7	12.5	12.8	18%
	4"	10	20.1	19.8	19.6	20.3	20%
		50	18.6	18.9	19.0	19.7	19%
		250	17.9	18.2	18.9	19.4	18%
	5"	10	24.3	24.7	23.7	24.0	19%
		50	23.9	24.0	24.1	24.3	19%
		250	23.7	23.8	23.9	24.0	19%
140	1"	10	2.7	2.5	2.7	2.6	10%
		50	2.4	2.2	2.3	2.4	9%
		250	2.1	2.0	2.0	2.9	9%
	2"	10	8.3	7.5	8.7	8.8	16%
		50	7.3	6.7	8.1	8.1	15%
		250	7.0	6.5	7.7	7.6	14%
	3"	10	10.7	10.4	9.1	9.3	13%
		50	9.8	9.2	9.1	9.0	12%
		250	9.4	8.7	8.7	8.8	12%
	4"	10	11.2	12.3	11.2	14.0	12%
		50	13.2	12.9	12.5	11.7	12%
		250	11.2	11.1	11.3	11.2	11%
	5"	10	18.8	17.6	17.5	17.7	14%
		50	17.3	17.3	17.3	17.5	14%
		250	17.1	17.2	17.3	17.1	14%

4-4 Discussion rod tests

The load-displacement curve for all quasi-static monotonic and cyclic tests follows a typical ductile steel path, see Figure 4-1. The cyclic curves match relatively well with the monotonic curves, showing no evidence of deteriorations or drop in the achievable peak load because of the cyclic loading. Image of the failed rod samples are presented Figure 4-4, the reduction in diameter at failure region signifies plastic necking, which is an evidence of ductile failure.

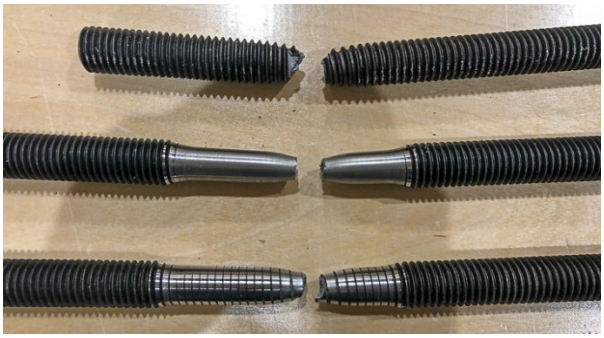

Figure 4-4: Failed rod after testing

The results, summarized in Table 4-5, show a consistent peak load F_{Peak} and yield load $F_{y,\,rod,}$ across all tested samples. A coefficient of variation (COV) of 2% was obtained. For design purposes using the full diameter samples, 95th percentile of 197kN was determined for peak load F_{Peak} and a 5th percentile of 162kN was calculated for yield load $F_{y,Rod}$ from the normal distribution of tested sample as shown Table 4-5.

As for the difference between the monotonic and cyclic test, the only difference worth mentioning is the elastic deformation. Samples tested under cyclic loading experienced a slightly larger deformation than samples tested under quasi-static monotonic loading in the elastic region. The peak load and deformation of results acquired from both tests showed no evidence a pinching. Therefore, the rod test shows no evidence of fatigue base on the result

attained. It is worth mentioning the performance of CLT. During the test, cracking sound from the CLT can be heard louder as the tensile load in the system increases, however, no visible crack was observed on the sample after the test. The steel rod had the ability to provide the necessary ductility. Across all tests, a ductility higher than 6 was achieved even though all samples failed at different elongations. Which signifies a highly ducting hold-down rod.

To ensure the rod remains elastic during the hold-down test, an estimated 5th percentile normal distribution of yield strength hold-down rod from Table 4-5 was factor by a R_dR_o value of 1.3 to ensure the test remains elastic at targeted load as described in equation 4-1. Base on the result, a target load of 120 was concluded.

$$F_{Target} \leq \frac{F_{y'Rod}}{R_dR_o} = \frac{162.7}{1.3} = 125.15kN \qquad (4\text{-}1)$$

Table 4-5: Design peak load F_{load} and yield load $F_{y,Rod}$

Label	F_{Peak}	$F_{y,Rod}$
	[kN]	[kN]
ROD TEST 1	196.3	170.5
ROD TEST 2	194.0	170.7
ROD TEST 3	192.0	167.5
F-ROD-140-1	194.2	170.0
F-ROD-140-2	195.1	169.8
F-ROD-140-3	194.6	168.6
A-full	183.8	162.0
B-full	193.3	171.4
C-full	186.3	163.5
D-full	196.8	170.9
5th Percentile	-	162.7
95th Percentile	196.6	-
COV	2%	2%

4-5 Discussion CLT tests

According to Figure 4-2, the load-displacement curve for all tested samples shows a linear behavior. Sudden load drop at peak load indicates brittle failure of the CLT. Various brittle failure modes were observed on all CLT samples. Figure 4-5 shows the failure pattern observed and photos of these failure modes are shown in Figure 4-6 and Figure 4-7.

The panels with 140 mm wide openings failed along the entire five layers of the sample. However, failure in the panel with 120mm and 90mm wide openings failed mostly on the first two layers on either side. Failure load for most samples was above 290kN, except for the 90-350-1 and 90-350-2 that failed at 177.8kN and 219.5kN respectively. This due to the smallest longitudinal edge distance a_l (see Figure 3-2). The result demonstrated that panel opening width do have an influence on load carrying capacity of the CLT, this is similar to the finding of Asgari et al. in his study [15]. Panel with opening width smaller than the width of the lamella, performed better that the wither sample with a less brittle failure mode.

Generally, to ensure the desired ductile failure for the hold-down, all other components was well capacity protected from the hold-down rod. From Table 3-5, it can be observed that the load bearing capacity of the rubber pad reduces as the thickness of the pad increases. For the 140mm rubber pad, the highest value of 341kN was estimated for the 1" thick pad, while the lowest load bearing capacity of 234kN was estimated in the 5" rubber pad. For the 90mm rubber pad, an estimate of 210kN and 148kN was recommended for the 1" and 5" rubber pad respectively. In deduction, one could argue that the 140mm MER hold-down is a more suitable solution because the estimated load bearing capacity of the 5" pad is higher than the normal distribution 95^{th} percentile for the peak load of the steel rod (see equation 4-2). For the CLT panel a minimum edge distance of 400mm was concluded as a result.

$$F_{peak} < F_{U,CLT} \text{ and } F_{U,rubber} \quad (4\text{-}2)$$

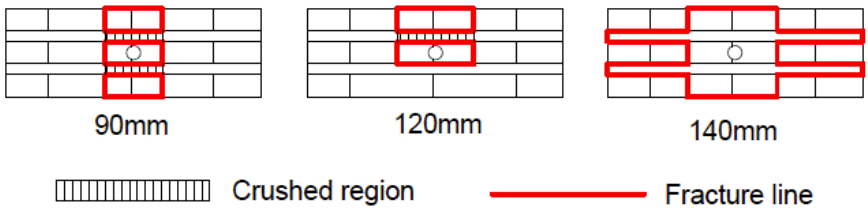

Figure 4-5: CLT failure patterns

Figure 4-6: CLT failed specimens, part 1

Figure 4-7: CLT failed specimens, part 2

4-6 Discussion hold-down tests

As for the performance of the CLT housing, the layout A form the hold-down layout causes early cracks on the CLT panel region beneath the rubber pad. This propagates as the number of tests carried out increases. Which subsequently lead to a premature failure of the outer lamellar of the CLT housing after three to four tests (see Figure 4-8a). The introduction of a base plate in layouts B and C resolved the issue completely. No visible cracks were observed

in all tests carried out using configuration B and C (see Figure 4-8b). All tests were completed using one CLT housing in either 90mm or 140mm rubber pad case. All hold-down layouts A, B and C (see Figure 3-10) produced similar results for the average load-displacement from the LVDTs attached to both sides of the CLT panel.

a)

b)

Figure 4-8: a) CLT failure of outer lamella using configuration A; b) CLT intact after multiple tests using configuration B

The load-deformation curves presented in Figure 4-3 follow a non-linear path to the targeted load as anticipated. The result also showed that rubber hold-down has low stiffness at the early loading stage, but its stiffness increases exponentially as the load increases. Rubber pad stiffness increases as the width of the rubber pad increases. The 90mm rubber pad deforms a lot more than the 140mm pad for any of the pad thicknesses. This demonstrated that pad width is a major contributing factor to the stiffness of rubber hold-down.

In Table 4-4, the average deformation for LVDT on both sides of each rubber pad is calculated for both top and bottom deformations and plotted in Figure 4-9. Overall, both 90mm and 140mm wide rubber pads exhibit an increase in horizontal deformation as the thickness of the rubber pad increases, which implies that using thicker rubber pad will reduce the stiffness of the hold-down. For individual rubber pad thickness, results demonstrate a slight decrease in average deformation as the loading rate increases. Its influence, however, is consistent for any rubber pad thickness. A difference of approximately 1mm was observed on an average for all loading rate irrespective of the rubber thickness. In translation, especially for high aspect ratio shearwall, the influence of loading rate on the story drift will be less than 1mm. This demonstrates that the influence of loading rate is negligible. The result in the Table also shows that at 120kN, the deformation achieved is less than 50% of the allowable recommended strain of 40% by the manufacturer's design guide specification. For example, it can be observed that the 90mm wide 5" thick rubber pad, produced strain deformation is less than 20% in experiment at target load, the estimated ultimate load capacity at 40% strain is 145kN.

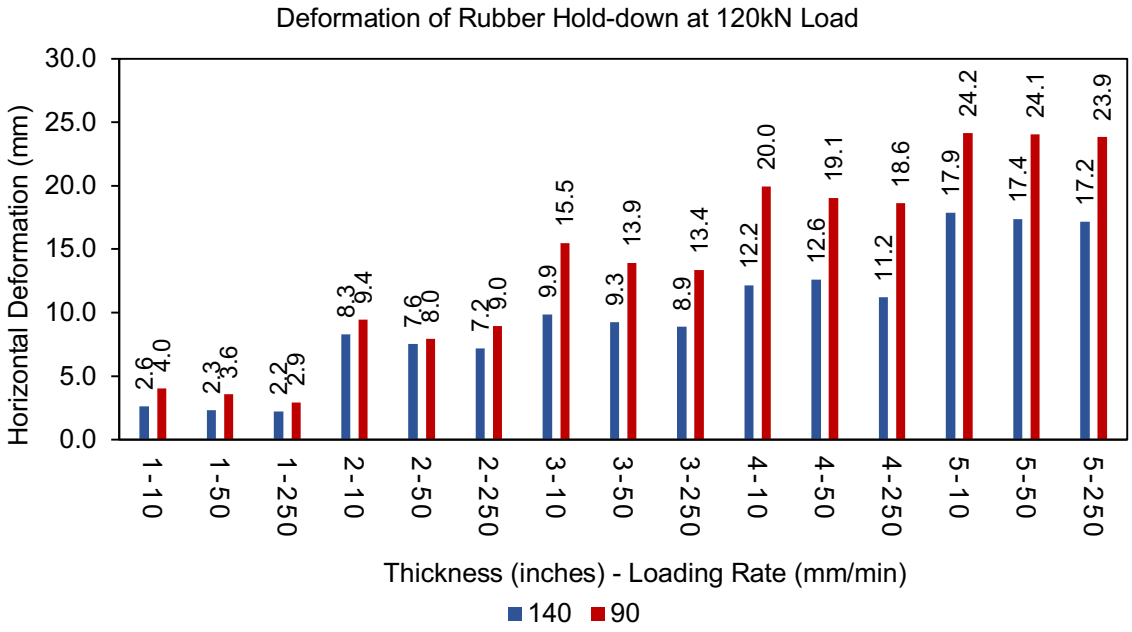

Figure 4-9: Deformation of hold-down at 120 kN load

In Figure 4-10, the relationship between mean deformation of the rubber pad at target load and shape factor (SF) of the rubber pad is illustrated. It demonstrated that shape factor is a major contributing factor to the stiffness of the rubber pad. As the SF increases, the attained deformation increases. This agrees with the findings of Asgari et al [15]. One must keep in mind that the SF is determined from the geometry of the rubber pad. When Figures 4-10a and Figure 4-10b are compared, it can be observed the, even though the SF trend looks similar, the deformation attained for the target load the 90mm wide rubber pad is higher than the 140mm wide rubber pad. This shows that surface area plays an explicit role in the relationship between the deformation of the rubber pad at target load, outside its relationship with SF. The curve fitting expression for rubber pad is illustrated in Equation 4-3. In addition to this, it is worth mentioning that the loading rate does not significantly contribute to the relation between deformation of the rubber pad and shape factor of the rubber pad.

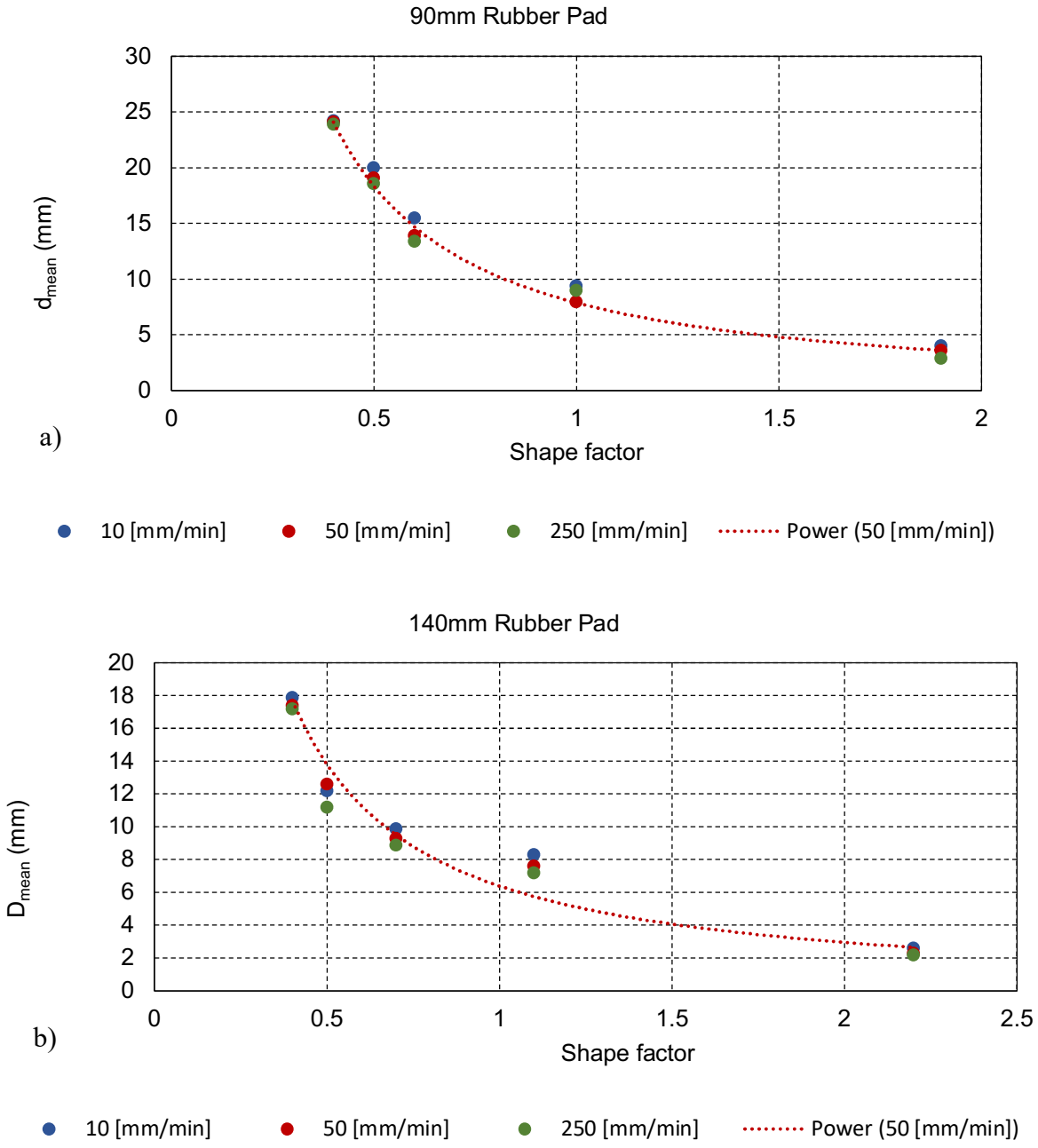

Figure 4-10: Hold-down deformation vs. shape factor under monotonic loading for a) 90mm and b) 140mm wide hold-downs

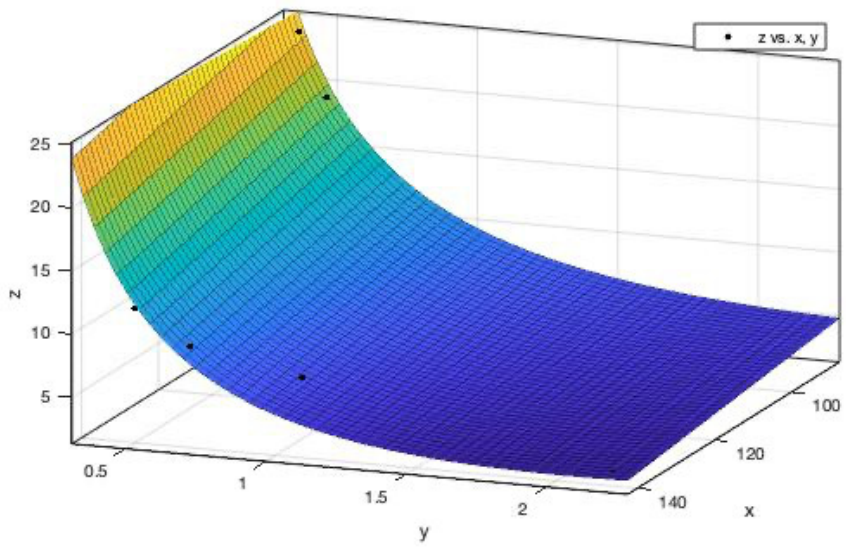

Figure 4-11: Hold-down deformation at 120kN vs shape function and width of rubber pad

The curve fitting expression for the relationship between shape function, d_{mean} and width of rubber pad at 120kN with a goodness of fit of $R^2 = 0.95$

$$d_{mean}@\,120kN = -0.0941w_R + 0.02228w_RSF + 15.57SF^{0.7228} \quad (4\text{-}3)$$

Where w_R is width of rubber and SF is the shape factor.

Chapter 5: Finite element analysis

5-1 Modell development

The shape factor (SF) has a significant influence on the stiffness of the hold-down [15]. The SF also has an influence on the allowable load bearing capacity of the rubber pad based on the empirical formula provided by the MER manufacturers design guide [33]. Figure 5-1 shows the contribution of shape factor on the allowable load bearing capacity of rubber pads based on estimation. One of the ways to improve the stiffness and load bearing capacity is to alter its SF. Since SF can be attributed to influencing the bulging behavior of a rubber pad, by altering the bulging behavior of the rubber to maintain a high shape factor, consequently improving the stiffness, and loaded bearing capacity of the rubber pad.

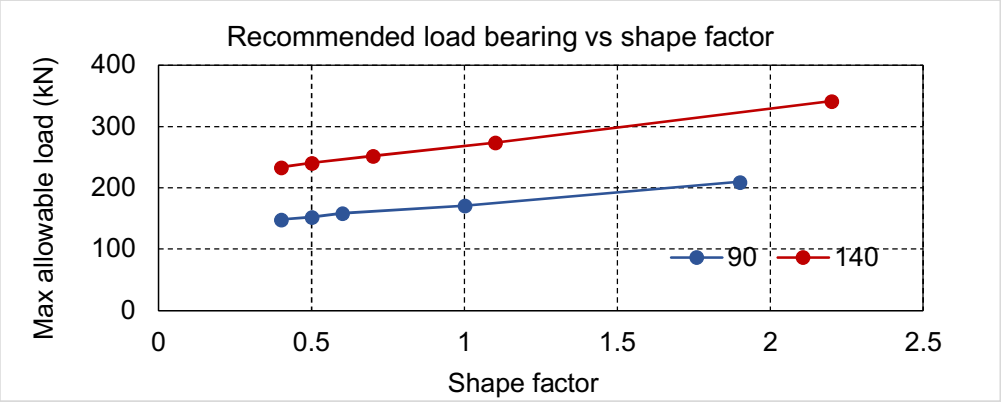

Figure 5-1: Maximum allowable load vs. shape factor

In the aim to optimize the hold-down system, a finite element model was developed using the hyperplastic properties developed by Asgari et al. [15]. A total of seven (7) simulations were carried out to produce a matching model of the tested sample and an optimized model of the existing hold-down concept. Two types of models were studied. The parametric data of the simulated tested sample is described in Figure 5-2 Table 5-1. In group 1, labeled NP2, NP3

and NP4, a full rectangular prism hyper-elastic rubber pad mode with no plate (NP = no plate) was modeled. In group 2, labeled P2, P3 and P4, include stacks of 1" rubber model with thin plate in-between each pad of the model to restrict bulging those that regions.

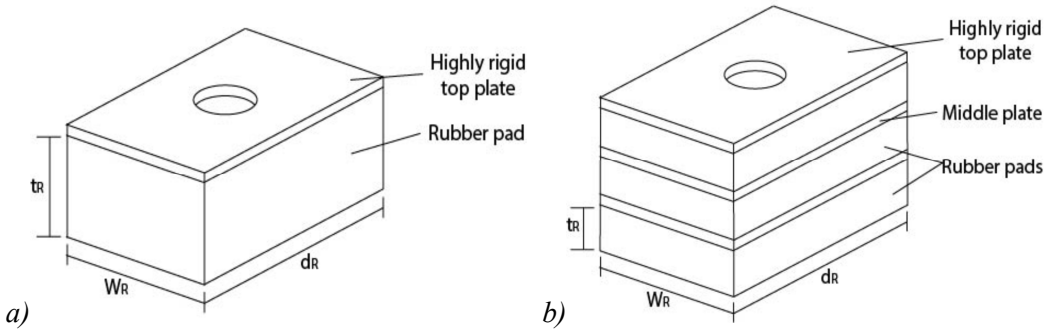

Figure 5-2: Sketch of the model with dimension definition

Table 5-1: The parametric data of the simulated sample

Label		d_R [mm]	w_R [mm]	t_R [inch]	N_R [mm]	$t_{R,t}$ [mm]	SF	V_{nr} KN
S1"	N/A	140	90	1	1	25.4	1.9	209.9
Group 1: hyper-elastic rubber pads with No plate glued between each pad								
NP2	No	140	90	2	1	50.8	1	171.4
NP3	No	140	90	3	1	76.2	0.6	158.6
NP4	No	140	90	4	1	101.6	0.5	152.2
Group 2: hyper-elastic rubber pads with plate glued between each pad								
P2"	yes	140	90	1	2	2"	1.9	209.9
P3"	yes	140	90	1	3	3"	1.9	209.9
P4"	yes	140	90	1	4	4"	1.9	209.9

The rubber pad was simulated using a Yeoh 3rd model with the parameter provided in Table 5-2. The model of P4 and NP4 are illustrated in Figure 5-5. Figure 5-4 on the other hand illustrates the contact interaction and boundary condition applied on the P4 and NP4 model. In

the models, deformation at the top was avoided, therefore, it was modeled as a fully rigid element. The middle plate, however, was modeled as linear elastic. Interaction between all members was assumed to be fully bonded. In other to avoid complexity of modelling frictional interaction with other members on the two long sides and at the middle hole of the rubber pad model, both regions were modeled as a frictionless support region. This also prevents bulging on the sides and on the middle hole. The bottom part of the model was modelled as a fully fixed in those regions. A nonlinear analysis was carried out on the model by applying a load of 120kN on the top plate.

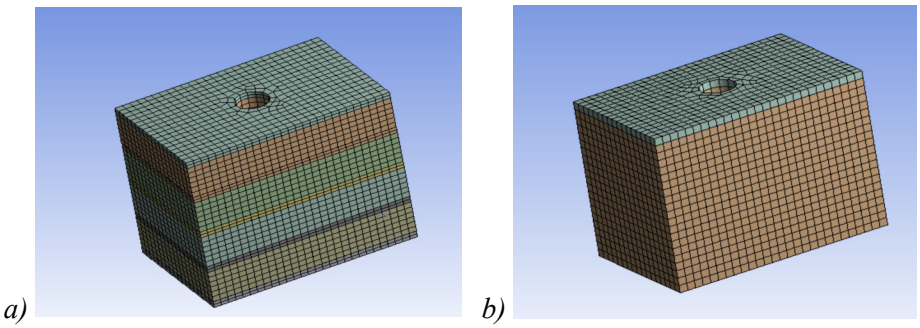

Figure 5-3: Finite element models a) P4 b) NP4

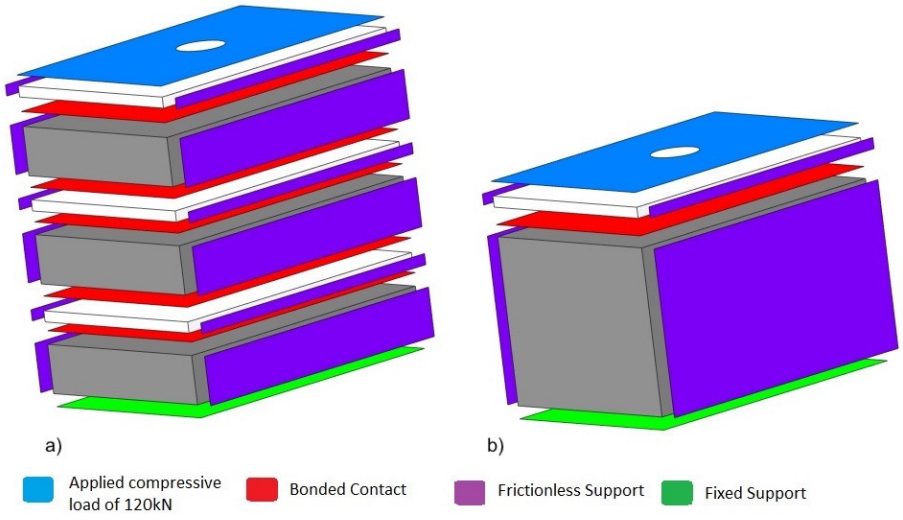

Figure 5-4: Model contact interaction and boundary condition

Table 5-2: Yeoh 3rd model parameters

Yeoh 3rd Order					
Material Constant			Incompressibility Parameter		
C10	C20	C30	D1	D2	D3
Pa	Pa	Pa	Pa^{-1}	Pa^{-2}	Pa^{-3}
1.36E+06	-2.27E+06	5.61E+06	2.90E-06	-1.71E-11	5.17E-11

5-2 FEA results and discussion

Based on the ANSYS simulation of the rubber pad. Figure 5-3a shows the deformed shape of the rubber pad after a load of 120kN is applied. Figure 5-3b on the other hand shows the deformed shape of the optimized 4-layer pad after being loaded. The result generated from that analysis is illustrated in Figure 5-4 to Figure 5-6.

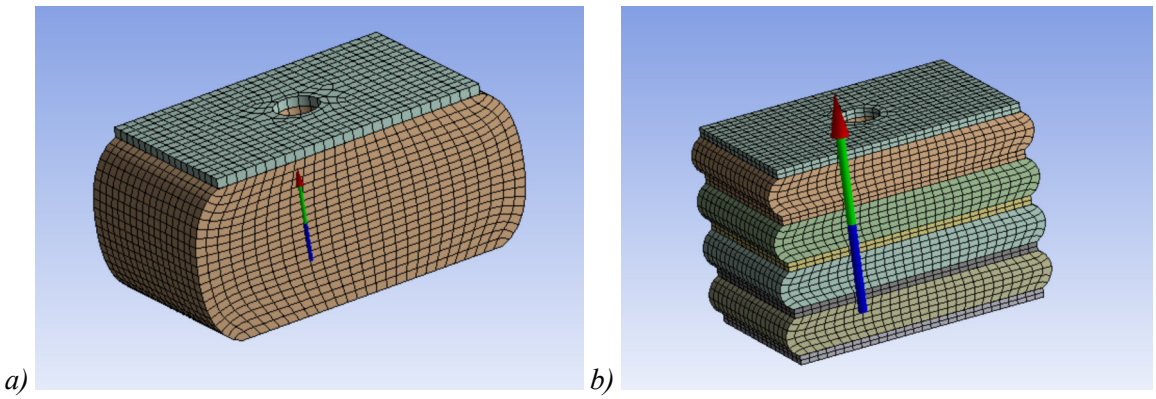

Figure 5-5: Simulated compression of the rubber pad of a) NP4, b) P4

Figure 5-6 shows the load-displacement curves of the numerical simulations. The curves follow a nonlinear path that is similar to the laboratory test results. An improved stiffness in the optimized model was achieved, P4 is stiffer than NP4 by approx. 40%. Figure 5-7 shows the relationship between the maximum displacement of both models at 120kN. The result shows a lower deformation in the pad model with lamellar when compared to the model with

laminated steel plate. The bulging pattern, when both types of samples are placed side by side shows that the shape factor of the steel plate laminated rubber pad is a lot closer to a 1" rubber pad shape factor irrespective of its thicknesses when this boundary condition is applied in each layer. Which in return means, an improved stiffness can be achieved by introducing a steel plate lamellar in between each rubber pad layer and also, using thinner rubber layer.

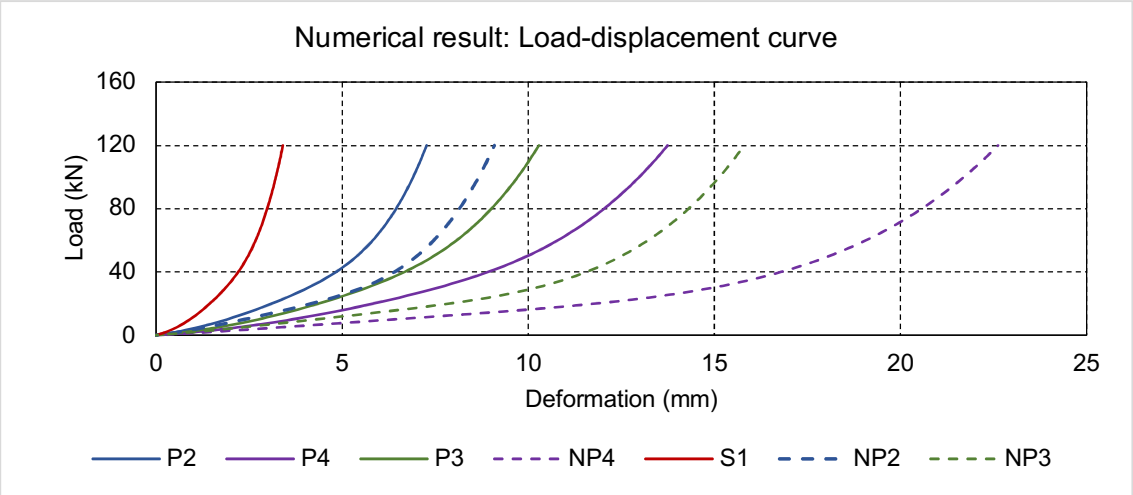

Figure 5-6: Simulated load-displacements

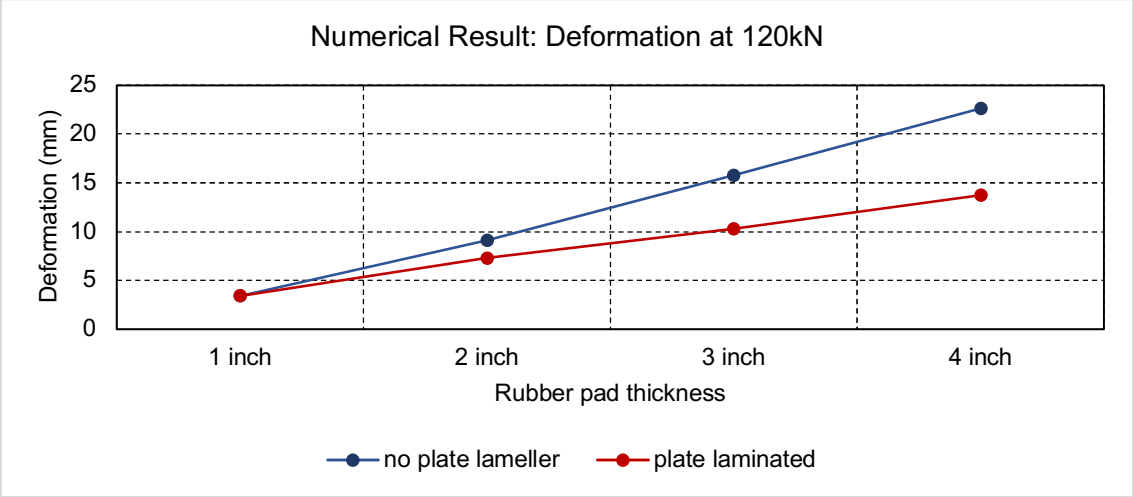

Figure 5-7: Deformation at 120kN based on numerical model

5-3 Verification

Model and experimental data are compared in Figure 5-8 to further verify the accuracy of the model. Based on comparison of the model with the experimental result; the model only worked for 1" (S1) and 2" (NP2) rubber pads, as the thickness of the rubber pad increased, the model began to lose its accuracy for the rubber pad simulation with no plate in between. This is because the frictionless contact applied on the sides of the mode is not an accurate model of rubber pad contact. In the experiment samples that the models are compared to, there is a frictional contact interaction between restricted long side of the rubber pad and the inner surface of the CLT wood panel. This was modeled as frictionless contact in the models to avoid numerical convergence problem. The margin of error carried becomes more pronounce as the thickness of the rubber pad increases due to shape factor. Although S1 and the 1" pad experimental data match more accurately, it is tough to tell how accurate the optimized rubber pad model simulation will be until an actual laboratory experiment is carried out.

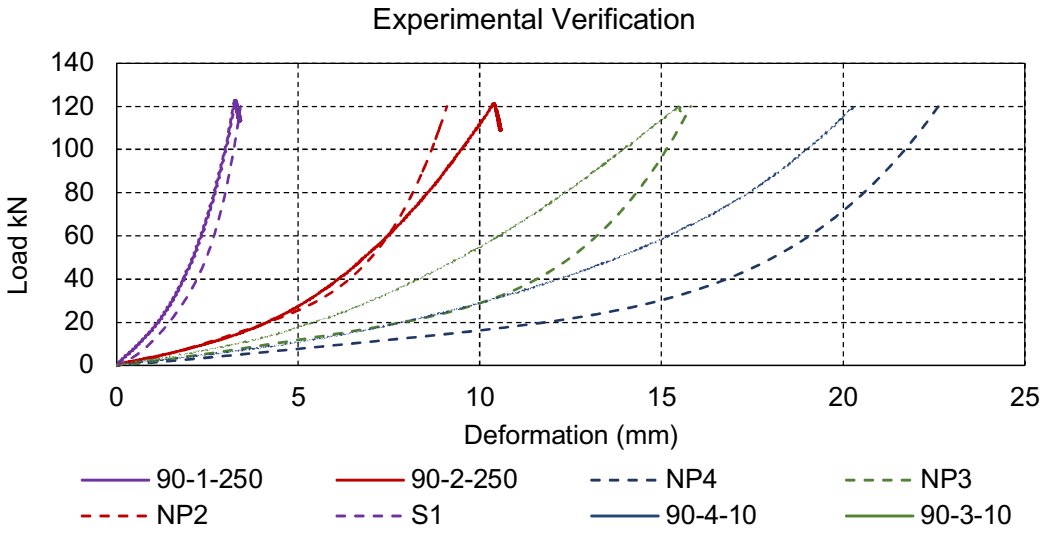

Figure 5-8: Numerical result verification

Chapter 6: Conclusions and outlook

The performance of a hyper-elastic high-capacity hold-down was investigated at the component level through tests on: i) hold-down steel rod; ii) CLT housing; and iii) hold-down assemblies with different sizes of rubber pads. These demonstrated that the hold-down assembly can achieve the performance as desired for CLT shearwall according to CSA 086-19. The hold-down system can remain elastic at 120kN without degrading and ductile failure can be achieved as long as the steel rod is the weakest link in the setup. The strength of the rod provided sufficient tolerance for elastic behavior of the hold-down even at higher load. For higher utilization of the concept, it is recommended that a stronger hold-down rod may be considered. However, all other members must be capacity protected to avoid brittle failure.

The tests further showed that the edge distance and the opening width are contributing factors to the CLT housing failure modes and ultimate load-carrying resistance. A precautionary minimum edge distance of 400mm or greater is recommended for the CLT housing. Further studies are required to fully understand individual parameter's significance.

The stiffness of shearwalls equipped with such hold-down will depend on the rubber pad dimensions and the resulting shape factor. Using thinner rubber increases the shape factor and consequently the hold-down stiffness. The rubber pad empirical formula provided in the manufacturer's design guide is highly conservative. Loading rate add minimal contributing factor to deformation based on result generated. The loaded surface area of the rubber pad is a major contributing factor in the load bearing capacity. But one must keep in mind that, the use of wider pad can weaken the CLT, thereby leaving it vulnerable to brittle failure.

The finite element simulations showed that, by introducing a middle plate glued between each rubber pad layer, the amount of deformation in the rubber pad can be highly reduced.

Based on findings, the following design approach is proposed: First, determine peak load F_{peak} and yield load $F_{y,rod}$ either through manufacturer guide or experiment. Second, calculate target elastic load limit F_{Target} by apply a reduction factor R_dR_o of 1.3 to the yield load $F_{y,rod}$. Third, ensure ultimate CLT load $F_{U,CLT}$ and F_{rubber} is greater than peak load $F_{peak.}$

The high-capacity hyper-elastic rubber hold-down has shown remarkable performance on the component level based on the test all carried out. A full scale shearwall is appropriate to fully understand the feasibility and performance of the concept.

References

[1] F. Wemer and F. Richter, "Wood: A Good Choice for Energy Efficiency and the Environment," *The International Journal of Life Cycle Assessment,* vol. 12, no. 7, pp. 470-479, 2007.

[2] BCTF, "Seismic mitigation: The urgent need for safer schools," October 2018. [Online]. Available: https://www.bctf.ca/publications/ResearchReports.aspx?id=52021.

[3] Ceccotti A., Follesa M., Kawai N., Lauriola M.P., Minowa C., Sandhaas C., Yasumura M. Which Seismic Behaviour Factor for Multi-Storey Buildings made of Cross-Laminated Wooden Panels? *Proceedings of the 39th CIB W18 Meeting*, paper 39-15-4, Firenze, 2006.

[4] Tamagnone, Gabriele & Rinaldin, Giovanni & Fragiacomo, Massimo. (2017). A novel method for non-linear design of CLT wall systems. Engineering Structures. 167. 10.1016/j.engstruct.2017.09.010.

[5] Ceccotti, A., Sandhaas, C., Okabe, M., Yasumura, M., Minowa, C. and Kawai, N. (2013), SOFIE project – 3D shaking table test on a seven-storey full-scale cross-laminated timber building. Earthquake Engng Struct. Dyn., 42: 2003-2021. https://doi.org/10.1002/eqe.2309

[6] Canadian Wood Council, "Tall wood building," 2021. [Online]. Available: https://cwc.ca/how-to-build-with-wood/building-systems/tall-wood-buildings/.

[7] Fragiacomo, Massimo & Dujic, Bruno & Sustersic, Iztok. (2011). Elastic and ductile design of multi-storey crosslam massive wooden buildings under seismic actions. Engineering Structures - ENG STRUCT. 33. 3043-3053. 10.1016/j.engstruct.2011.05.020.

[8] Iqbal, Prestressed timber structures for multi-storied buildings: from theory to practice, *Resilient Infrastructure*, University of Northern British Columbia, Canada, 2016.

[9] Pozza, L., Saetta, A., Savoia, M., & Talledo, D. (2018). Angle bracket connections for CLT structures: Experimental characterization and numerical modelling. *Construction and Building Materials, 191*, 95-113.

[10] Pozza, L., Ferracuti, B., Massari, M., & Savoia, M. (2018). Axial – Shear interaction on CLT hold-down connections – Experimental investigation. *Engineering Structures, 160*, 95-110.

[11] British Standard, "BS EN 12512:2001 - Timber structures — Test methods — Cyclic testing of joints made with mechanical fasteners," BSi British Standard, 2005.

[12] Popovski, M., Karacabeyli, E., Ceccotti, A. 2011. Seismic Performance of Cross-Laminated Timber Buildings. Chapter 4 of the Handbook on Cross-Laminated Timber. FPInnovations Special Publication SP-528E, ISBN 978-0-86488-547-0.

[13] National Standard of Canada, CSA O86:19. 2019. Canadian Standards Association Standard O86 - Engineering Design in Wood. CSA, Mississauga, Ontario, Canada.

[14] Trutalli, D., Marchi, L., Scotta, R. *et al.* Capacity design of traditional and innovative ductile connections for earthquake-resistant CLT structures. *Bull Earthquake Eng* **17,** 2115–2136 (2019). https://doi.org/10.1007/s10518-018-00536-6

[15] Asgari, Hosein & Tannert, Thomas & Ebadi, Mohammad Mehdi & Loss, Cristiano & Popovski, Marjan. (2021). Hyperelastic hold-down solution for CLT shear walls. Construction and Building Materials. 289. 123173. 10.1016/j.conbuildmat.2021.123173.

[16] Erol Karacabeyli, Sylvain Gagnon & FPInnovations, Canadian CLT Handbook, 2019 Edition. Volume 1, FPInnovations, 2019.

[17] Brandner, Reinhard & Dietsch, Philipp & Dröscher, Julia & Schulte-Wrede, Michael & Kreuzinger, Heinrich & Sieder, Mike. (2017). Cross laminated timber (CLT) diaphragms under shear: Test configuration, properties and design. Construction and Building Materials. 147. 312-327. 10.1016/j.conbuildmat.2017.04.153.

[18] Popovski M. Pavric I. and Schneider J. (2014). Performance of two-storey CLT house subjected to lateral loads, Quebec.

[19] G. Katie, "Architect Magazine," Zonda Media, 27 July 2009. [Online]. Available: https://www.architectmagazine.com/technology/detail/murray-grove-wood-framed-high-rise_o. [Accessed 12 June 2021].

[20] Connolly, T., Loss, C., Iqbal, A., & Tannert, T. (2018). Feasibility Study of Mass-Timber Cores for the UBC Tall Wood Building. *Buildings, 8*, 98.

[21] Canadian wood council, wood design manual, vol. 1, Ottawa, ON: Canadian wood council, 2017.

[22] Izzi, Matteo & Polastri, Andrea & Fragiacomo, Massimo. (2018). Investigating the Hysteretic Behavior of Cross-Laminated Timber Wall Systems due to Connections. Journal of Structural Engineering. 144. 10.1061/(ASCE)ST.1943-541X.0002022.

[23] Shahnewaz, Md & Popovski, Marjan & Tannert, Thomas. (2019). Resistance of Cross-Laminated Timber Shear Walls for Platform-Type Construction. Journal of Structural Engineering. 145. 10.1061/(ASCE)ST.1943-541X.0002413.

[24] Izzi, Matteo & Casagrande, Daniele & Bezzi, Stefano & Pasca, Dag Pasquale & Follesa, Maurizio & Tomasi, Roberto. (2018). Seismic behaviour of Cross-Laminated Timber structures: A state-of-the-art review. Engineering Structures. 170. 10.1016/j.engstruct.2018.05.060.

[25] Casagrande, Daniele & Rossi, Simone & Sartori, Tiziano & Tomasi, Roberto. (2015). Proposal of an analytical procedure and a simplified numerical model for elastic response of single-storey timber shear-walls. Construction and Building Materials. 102. 10.1016/j.conbuildmat.2014.12.114.

[26] G. Rinaldin, M. Fragiacomo, Non-linear simulation of shaking-table tests on 3- and 7-storey X-Lam timber buildings, Engineering Structures, Volume 113, Pages 133-148, (2016) https://doi.org/10.1016/j.engstruct.2016.01.055.

[27] Muñoz, W. and A. Salenikovich. “Determination of yield point and ductility of timber assemblies : in search for a harmonised approach.” (2008).

[28] Nolet, Vincent & Casagrande, Daniele & Doudak, Ghasan. (2019). Multipanel CLT shearwalls: an analytical methodology to predict the elastic-plastic behaviour. Engineering Structures. 179. 640-654. 10.1016/j.engstruct.2018.11.017.

[29] Ugalde, D., Almazán, J.L., Santa María, H. *et al.* Seismic protection technologies for timber structures: a review. *Eur. J. Wood Prod.* **77,** 173–194 (2019). https://doi.org/10.1007/s00107-019-01389-9

[30] Trutalli, D., Marchi, L., Scotta, R. *et al.* Capacity design of traditional and innovative ductile connections for earthquake-resistant CLT structures. *Bull Earthquake Eng* **17,** 2115–2136 (2019). https://doi.org/10.1007/s10518-018-00536-6

[31] Zhang, Xiaoyue & Shahnewaz, Md & Tannert, Thomas. (2018). Seismic reliability analysis of a timber steel hybrid system. Engineering Structures. 167. 10.1016/j.engstruct.2018.04.051.

[32] Amini, M & Lindt, John & Rammer, Douglas & Pei, Shiling & Line, Philip & Popovski, Marjan. (2018). Systematic experimental investigation to support the development of seismic performance factors for cross laminated timber shear wall systems. Engineering Structures. 172. 392-404. 10.1016/j.engstruct.2018.06.021.

[33] Masticord Structural Bearing pad, Design Guide third edition, VI, Inc., Illinois, USA: JVI Inc, the Bearing pad people, 1985.

[34] ASTM E 2126-09. Standard Test Methods for Cyclic (Reversed) Load Test for Shear Resistance of Vertical Elements of the Lateral Load Resisting Systems for Buildings. ASTM International, West Conshohocken, PA, US.

Appendix: All hold-down test result

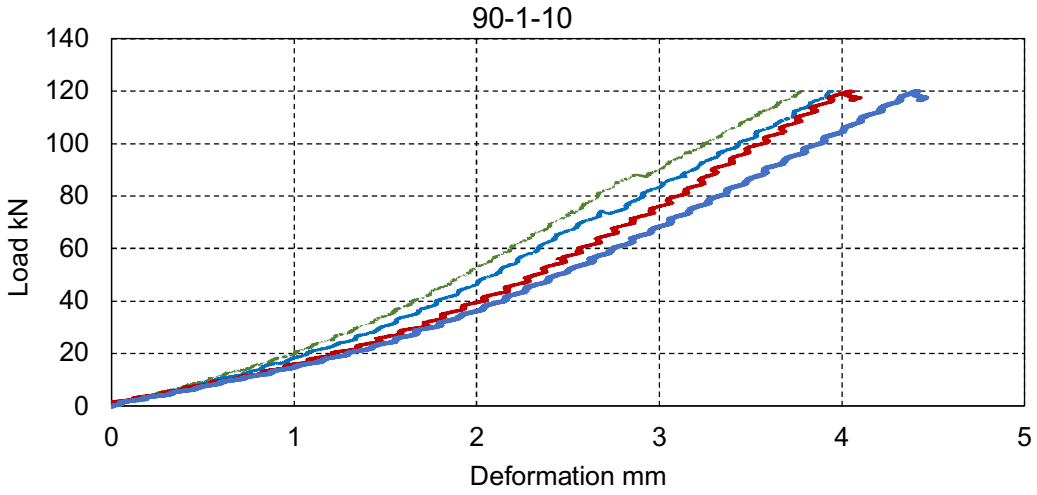

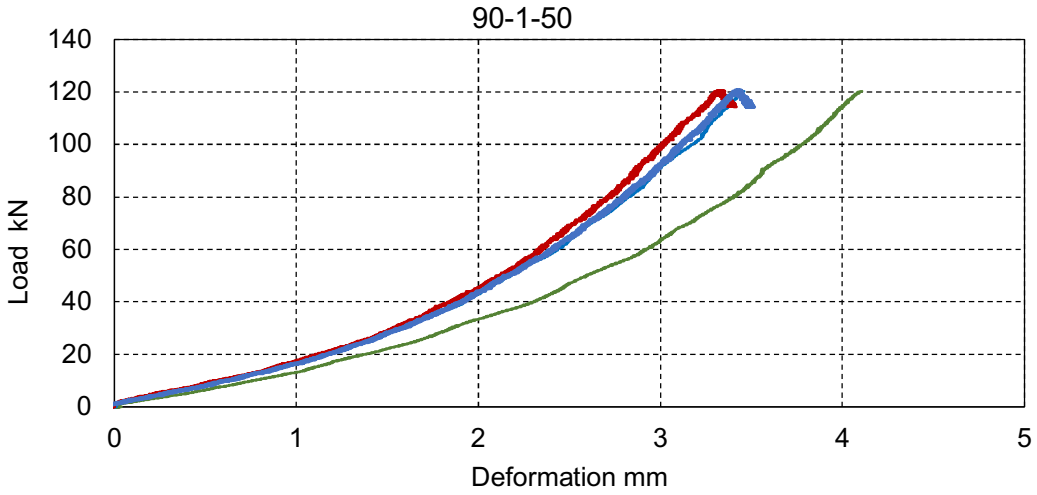

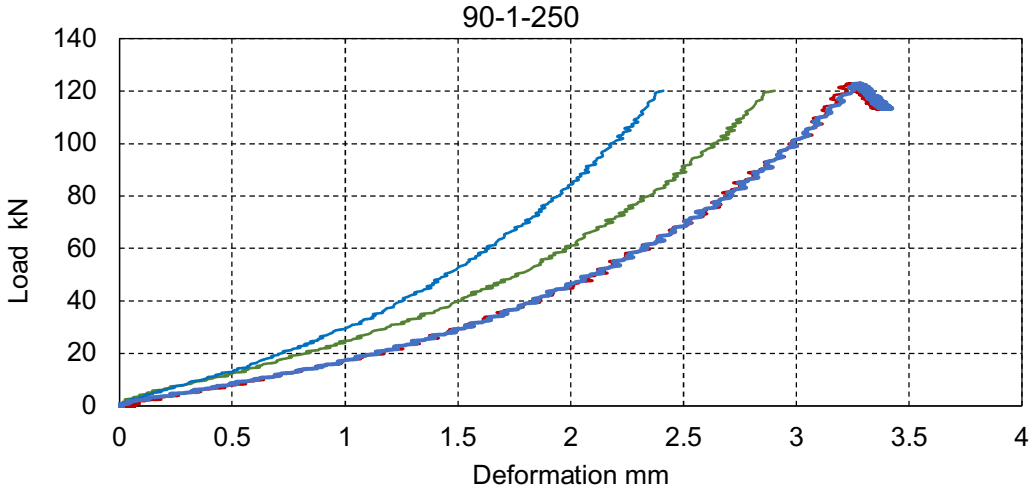
90-1-250
Load kN
Deformation mm
0
20
40
60
80
100
120
140
0
0.5
1
1.5
2
2.5
3
3.5
4

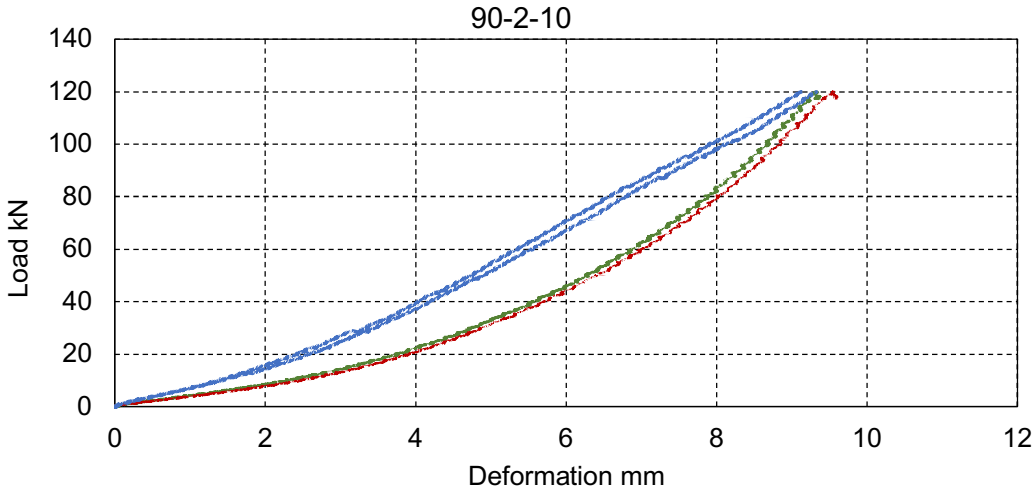
90-2-10
Load kN
Deformation mm
0
20
40
60
80
100
120
140
0
2
4
6
8
10
12

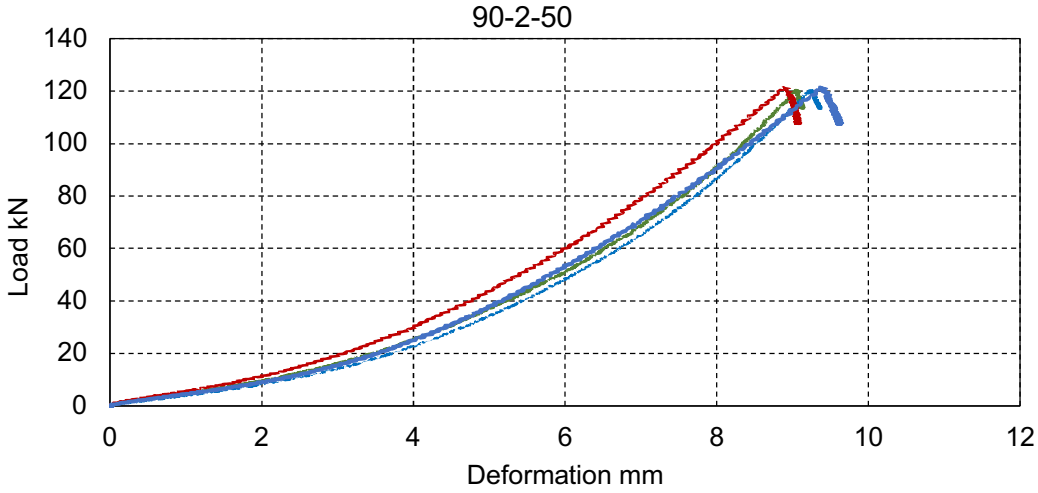
90-2-50
140
120
100
80
60
40
20
0
Load kN
0
2
4
6
8
10
12
Deformation mm

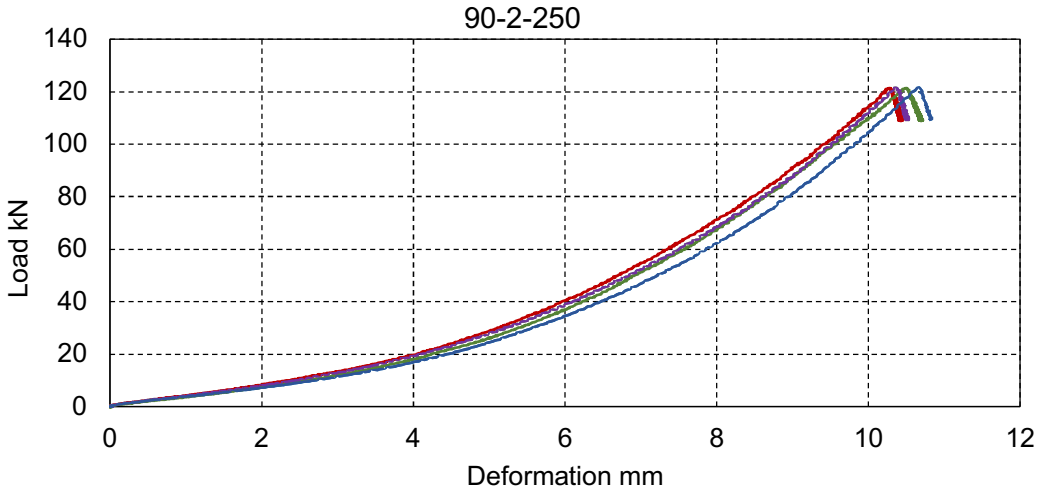
90-2-250
140
120
100
80
60
40
20
0
Load kN
0
2
4
6
8
10
12
Deformation mm

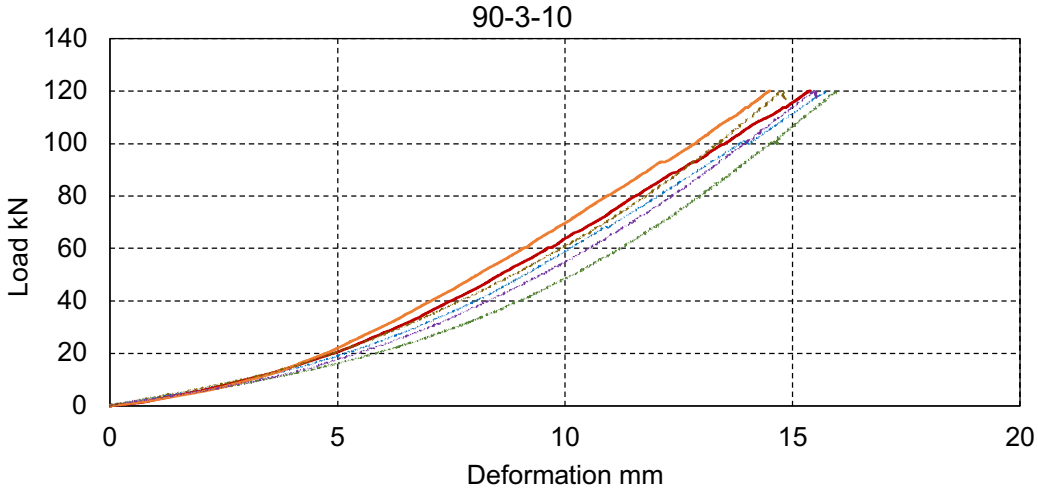
90-3-10
140
120
100
80
60
40
20
0
Load kN
0
5
10
15
20
Deformation mm

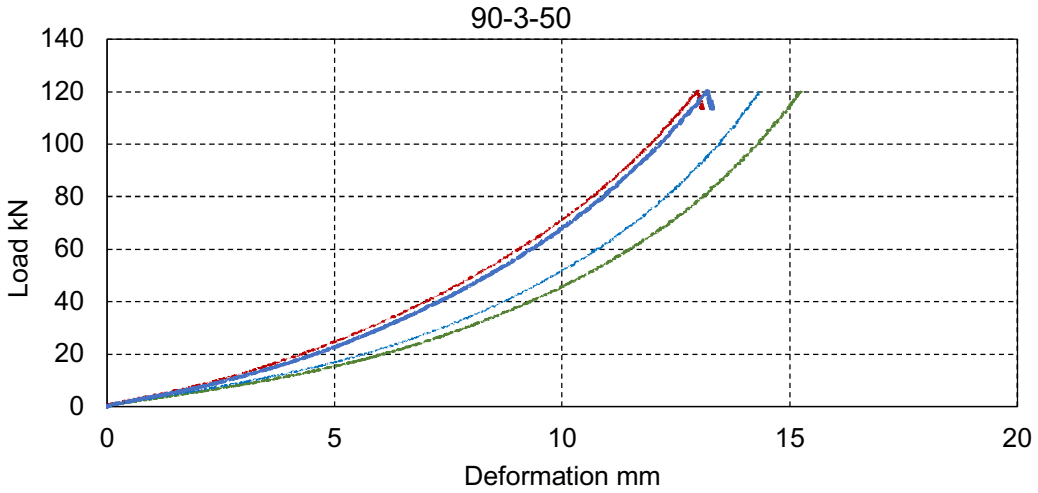
90-3-50
140
120
100
80
60
40
20
0
Load kN
0
5
10
15
20
Deformation mm

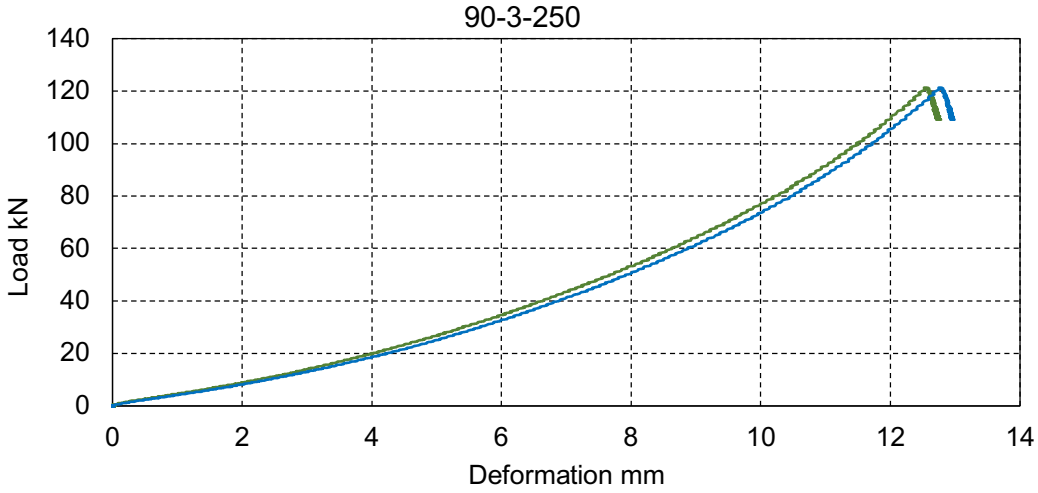
90-3-250
Load kN
Deformation mm
0
20
40
60
80
100
120
140
0
2
4
6
8
10
12
14

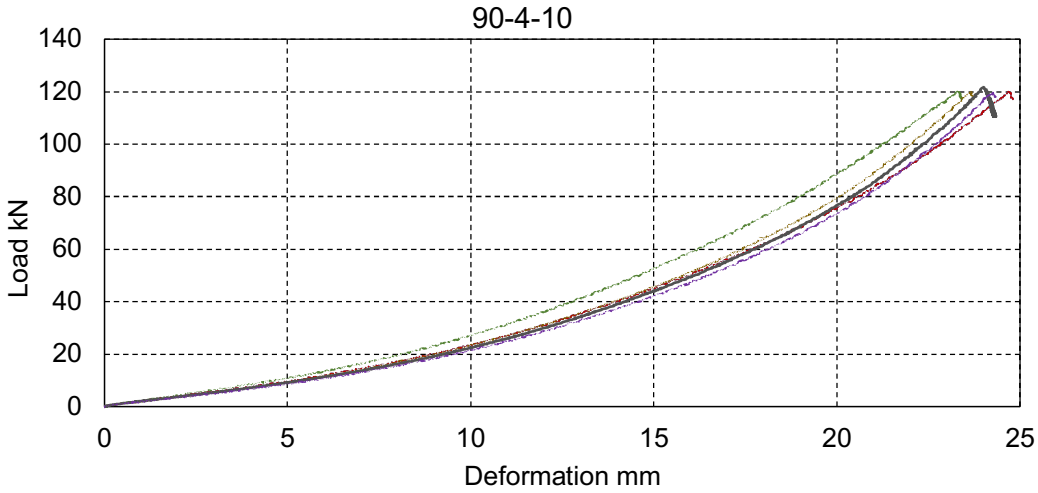
90-4-10
Load kN
Deformation mm
0
20
40
60
80
100
120
140
0
5
10
15
20
25

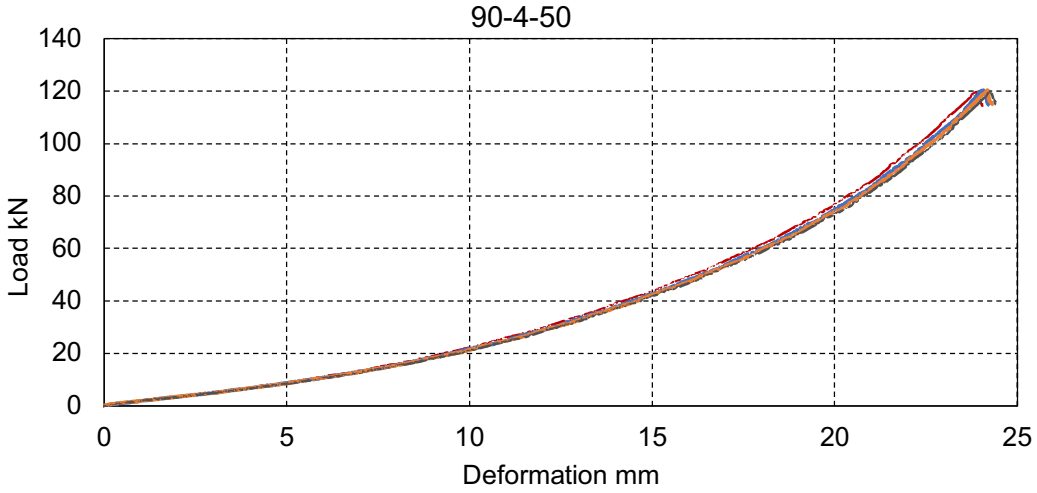
90-4-50
140
120
100
80
60
40
20
0
Load kN
0
5
10
15
20
25
Deformation mm

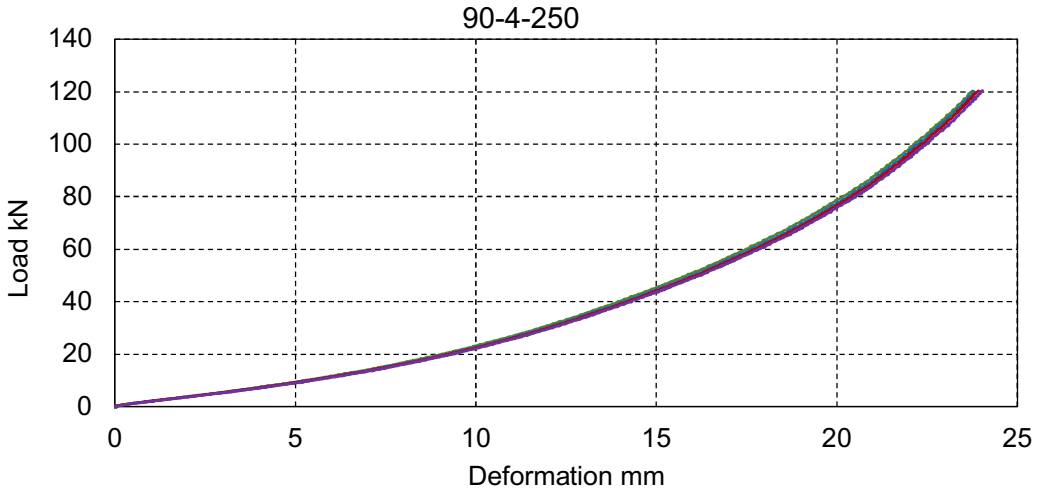
90-4-250
140
120
100
80
60
40
20
0
Load kN
0
5
10
15
20
25
Deformation mm

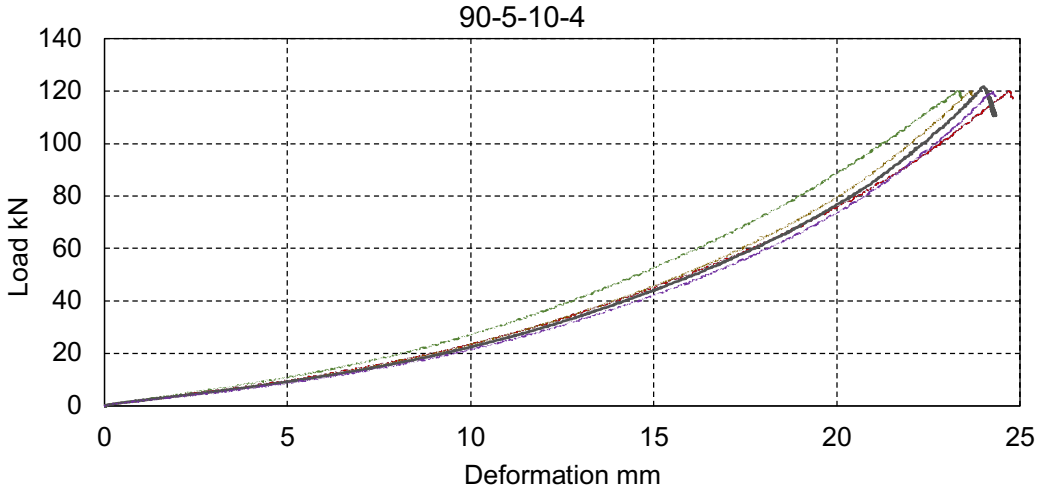
90-5-10-4
140
120
100
80
60
40
20
0
Load kN
0
5
10
15
20
25
Deformation mm

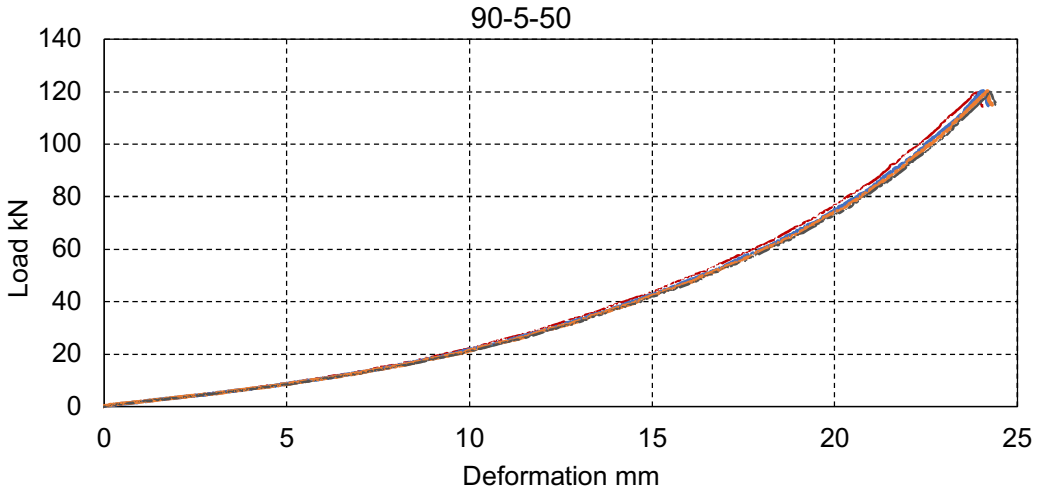
90-5-50
140
120
100
80
60
40
20
0
Load kN
0
5
10
15
20
25
Deformation mm

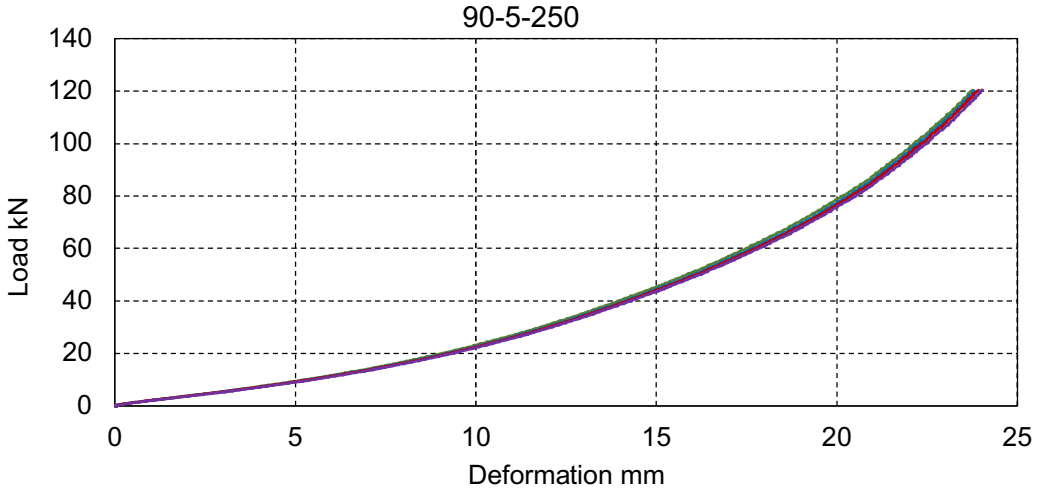
90-5-250
140
120
100
80
60
40
20
0
Load kN
0
5
10
15
20
25
Deformation mm

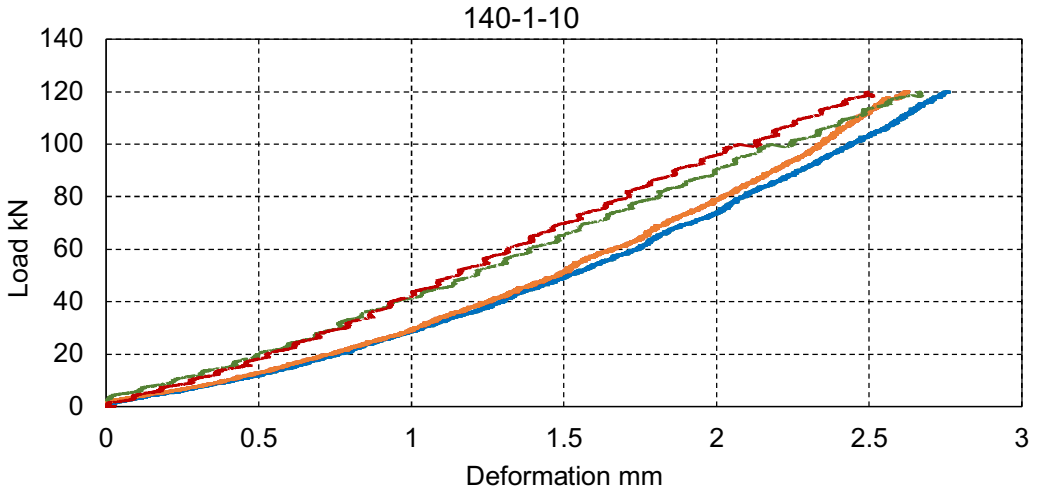
140-1-10
140
120
100
80
60
40
20
0
Load kN
0
0.5
1
1.5
2
2.5
3
Deformation mm

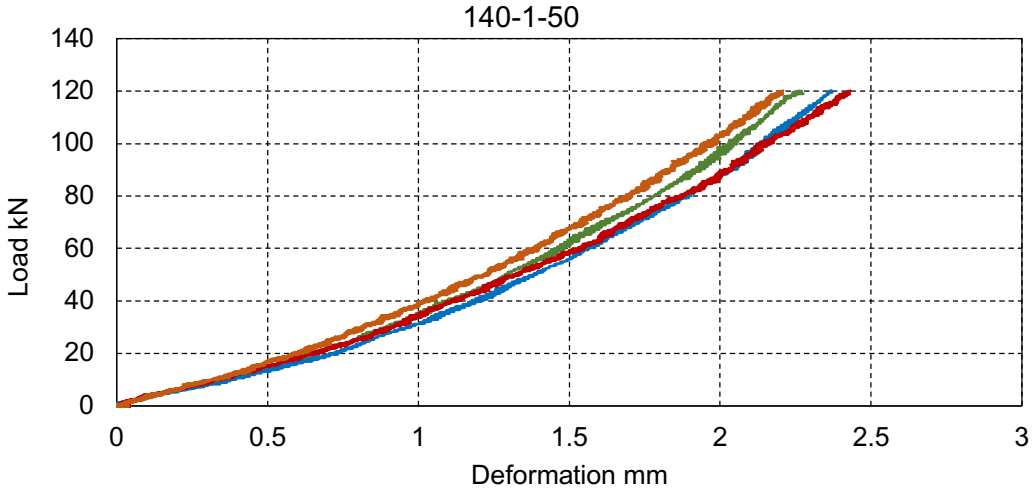
140-1-50
140
120
100
80
60
40
20
0
Load kN
0
0.5
1
1.5
2
2.5
3
Deformation mm

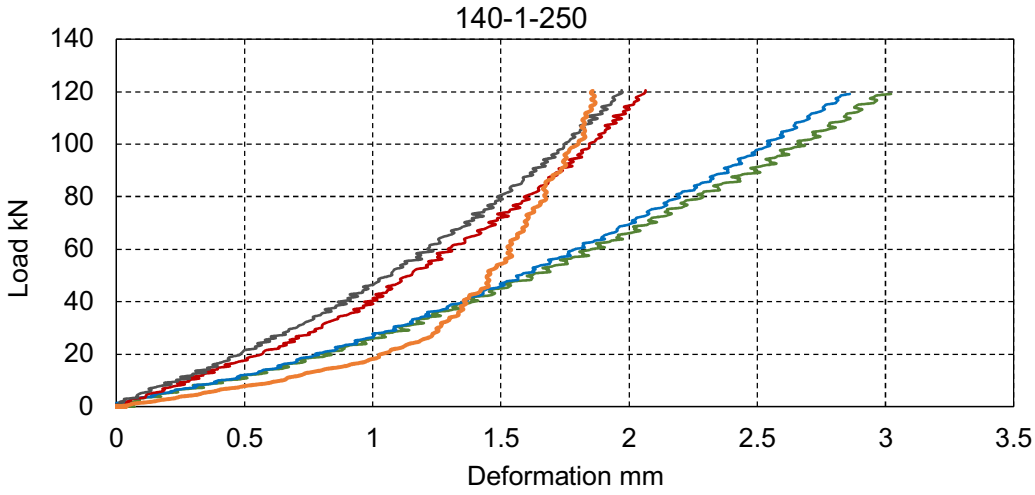
140-1-250
140
120
100
80
60
40
20
0
Load kN
0
0.5
1
1.5
2
2.5
3
3.5
Deformation mm

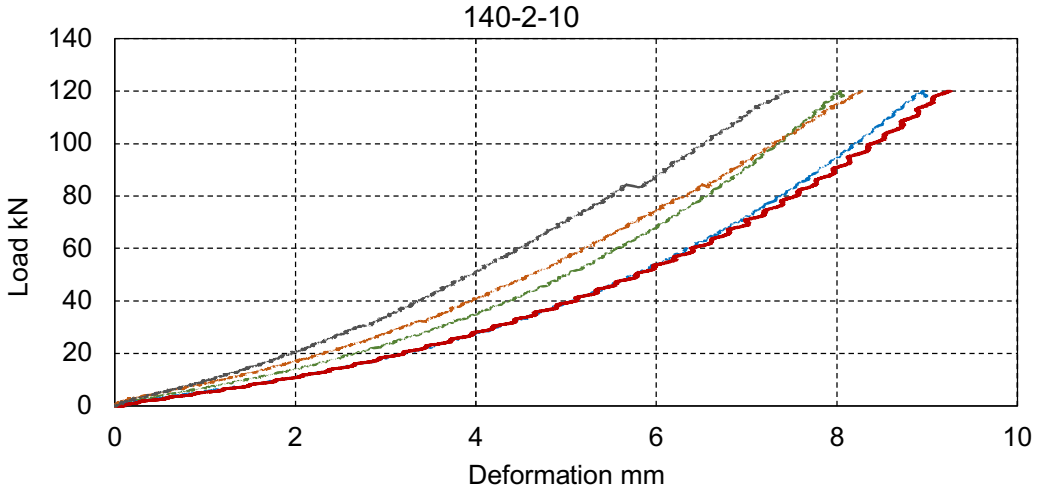
140-2-10
Load kN
Deformation mm
0
20
40
60
80
100
120
140
0
2
4
6
8
10

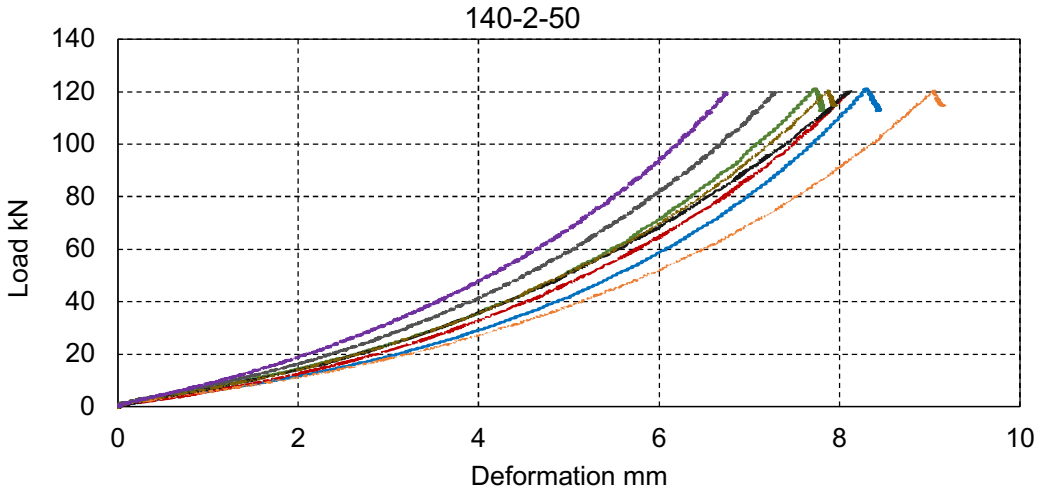
140-2-50
Load kN
Deformation mm
0
20
40
60
80
100
120
140
0
2
4
6
8
10

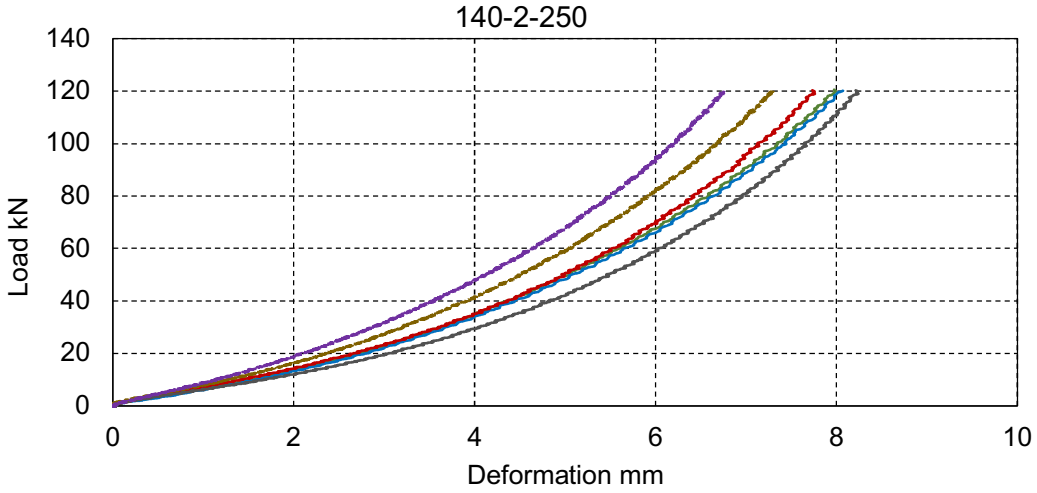
140-2-250
Load kN
Deformation mm
0
20
40
60
80
100
120
140
0
2
4
6
8
10

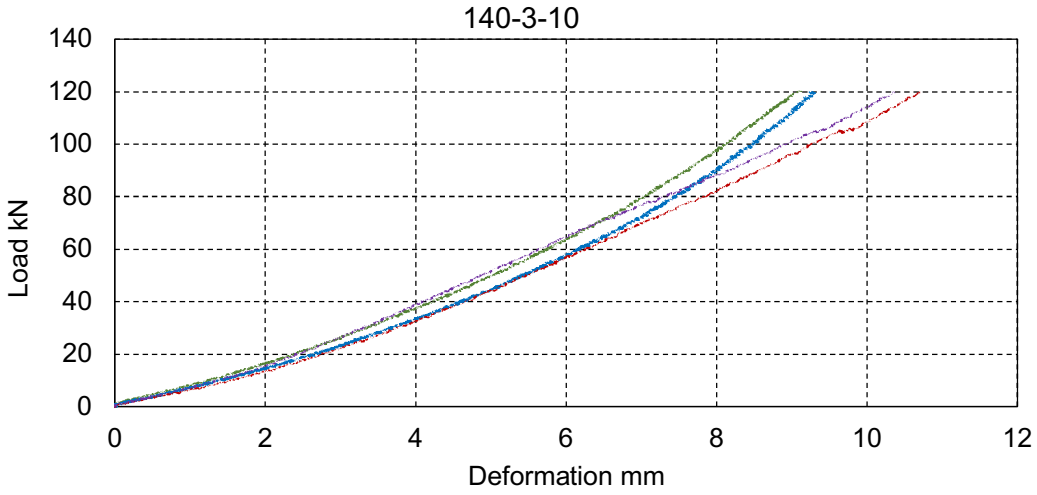
140-3-10
Load kN
Deformation mm
0
20
40
60
80
100
120
140
0
2
4
6
8
10
12

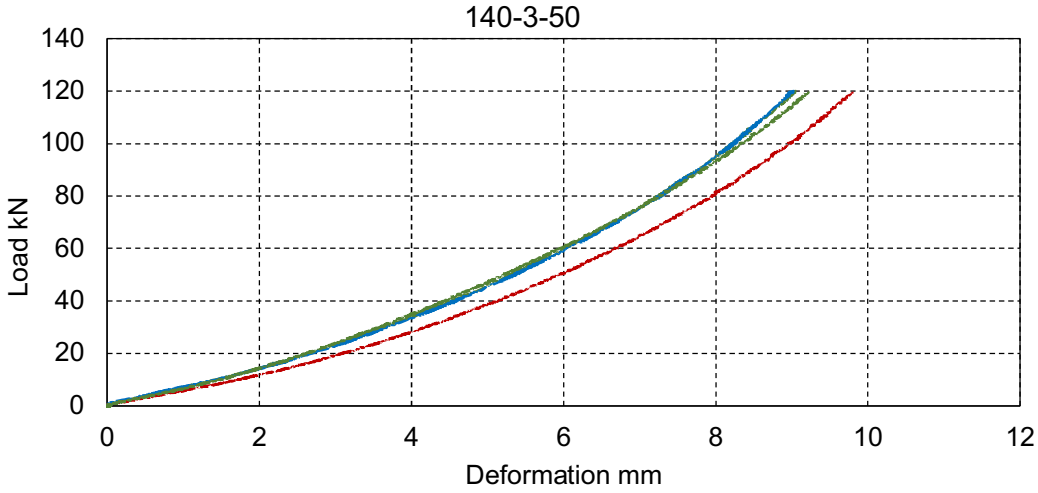
140-3-50
Load kN
Deformation mm
0
20
40
60
80
100
120
140
0
2
4
6
8
10
12

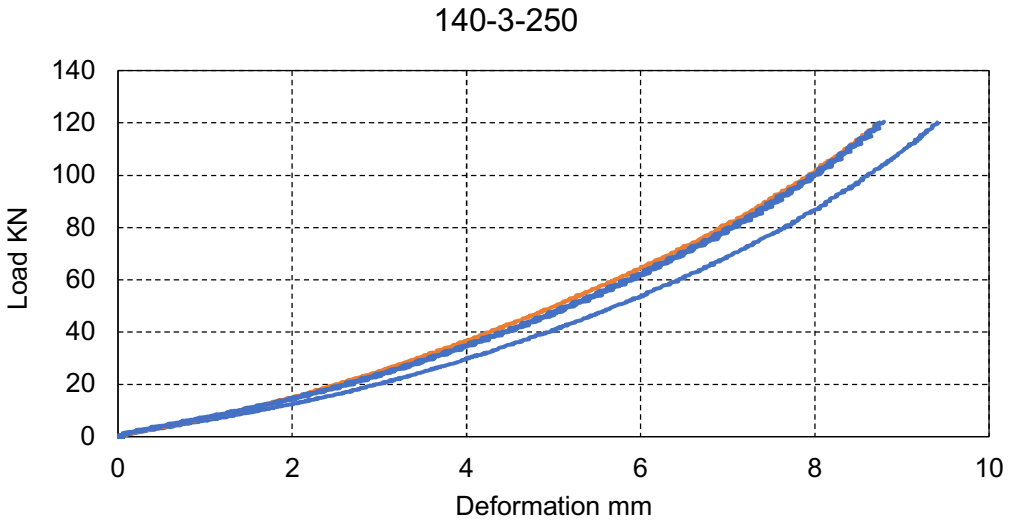
140-3-250
Load KN
Deformation mm
0
20
40
60
80
100
120
140
0
2
4
6
8
10

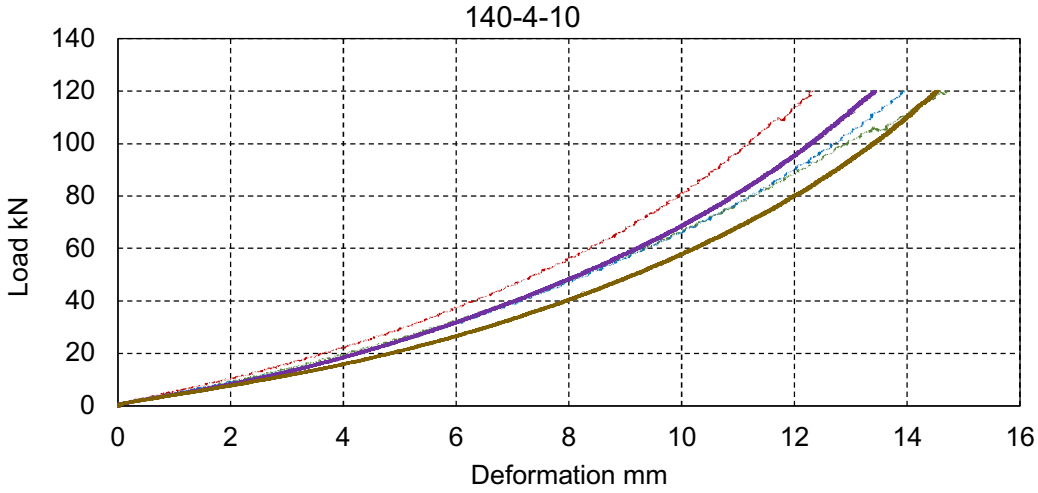
140-4-10
Load kN
Deformation mm
0
20
40
60
80
100
120
140
0
2
4
6
8
10
12
14
16

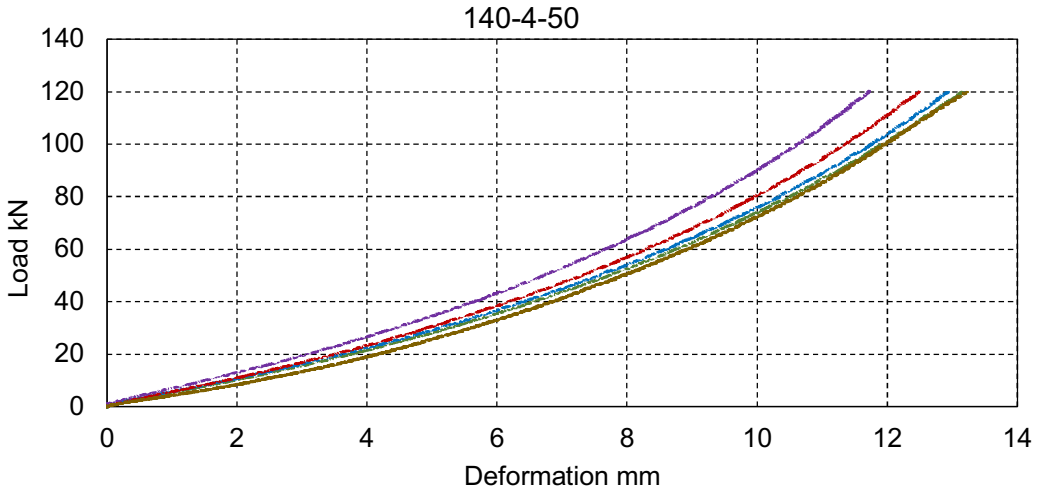
140-4-50
Load kN
Deformation mm
0
20
40
60
80
100
120
140
0
2
4
6
8
10
12
14

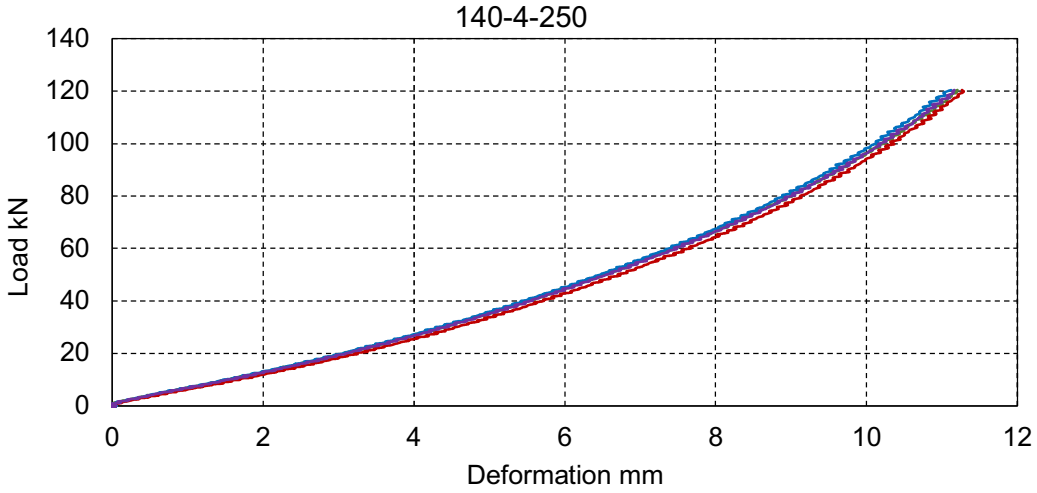
140-4-250
Load kN
Deformation mm
0
20
40
60
80
100
120
140
0
2
4
6
8
10
12

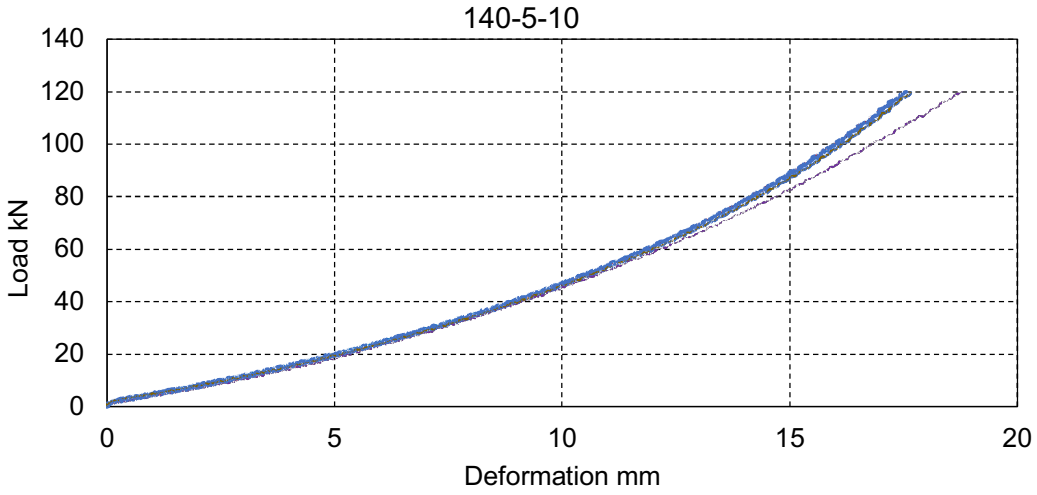
140-5-10
Load kN
Deformation mm
0
20
40
60
80
100
120
140
0
5
10
15
20

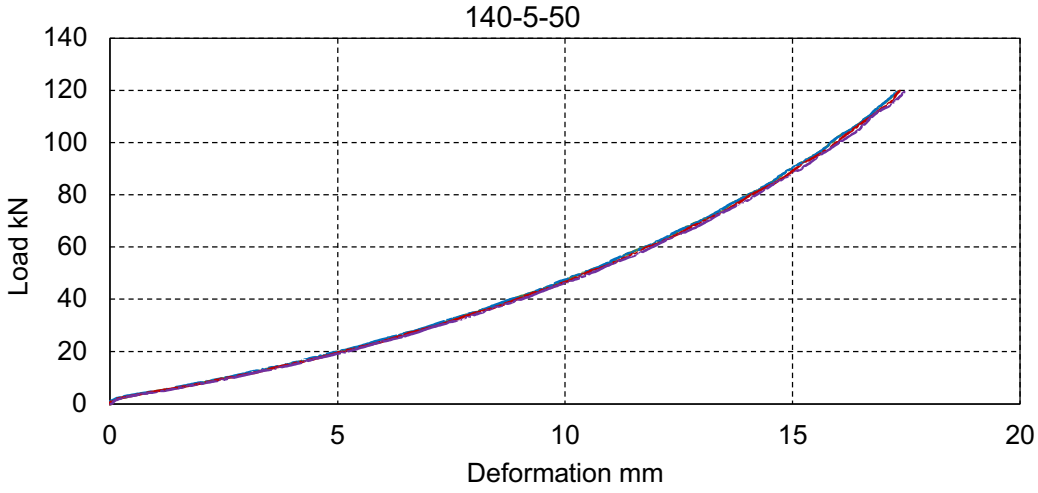
140-5-50
140
120
100
80
60
40
20
0
Load kN
0
5
10
15
20
Deformation mm

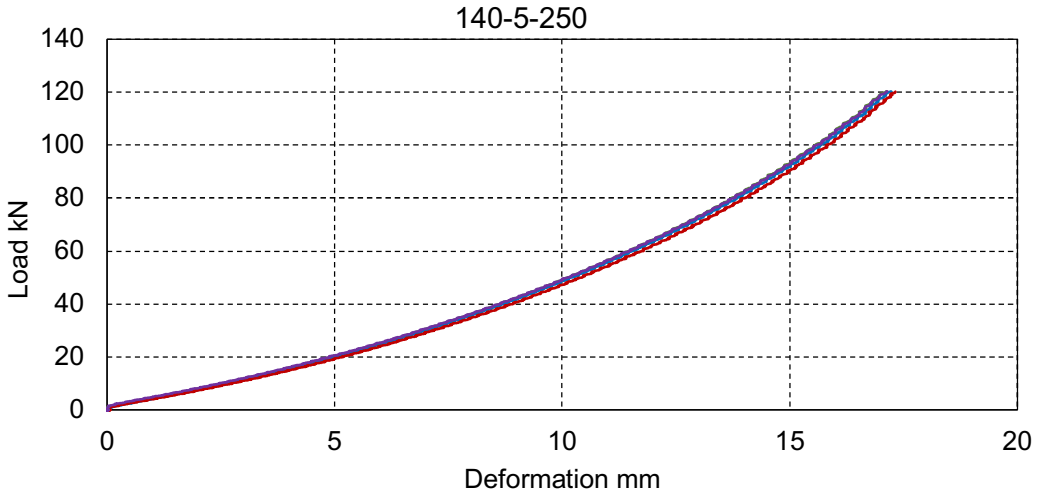
140-5-250
140
120
100
80
60
40
20
0
Load kN
0
5
10
15
20
Deformation mm